# Do Semiclassical Trajectory Theories Provide an Accurate Picture of Radiationless Decay for Systems with Accessible Surface Crossings?

**Michael D. Hack,[†] Ahren W. Jasper,[†] Yuri L. Volobuev,[†] David W. Schwenke,[‡] and Donald G. Truhlar*,[†]**

*Department of Chemistry and Supercomputer Institute, University of Minnesota, Minneapolis, Minnesota 55455-0431, and NASA Ames Research Center, Mail Stop 230-3, Moffett Field, California 94035-1000*

*Received: September 20, 1999; In Final Form: October 27, 1999*

We present quantum mechanical and semiclassical calculations of Feshbach funnel resonances that correspond to long-lived exciplexes in the $\tilde{A}\ ^2B_2$ state of $NaH_2$. These exciplexes decay to the ground state, $\tilde{X}\ ^2A_1$, by a surface crossing in $C_{2v}$ geometry. The quantum mechanical lifetimes and the branching probabilities for competing decay mechanisms are computed for two different $NaH_2$ potential energy matrices, and we explain the results in terms of features of the potential energy matrices. We compare the quantum mechanical calculations of the lifetimes and the average vibrational and rotational quantum numbers of the decay product, $H_2$, to two kinds of semiclassical trajectory calculations: the trajectory surface hopping method and the Ehrenfest self-consistent potential method (also called the time-dependent self-consistent field method). The trajectory surface hopping calculations use Tully's fewest switches algorithm and two different prescriptions for adjusting the momentum during a hop. Both the adiabatic and the diabatic representations are used for the trajectory surface hopping calculations. We show that the diabatic surface hopping calculations agree better with the quantum mechanical calculations than the adiabatic surface hopping calculations or the Ehrenfest calculations do for one potential energy matrix, and the adiabatic surface hopping calculations agree best with the quantum mechanical calculations for the other potential energy matrix. We test three criteria for predicting which representation is most accurate for surface hopping calculations. We compare the ability of the semiclassical methods to accurately reproduce the quantum mechanical trends between the two potential matrices, and we review other recent comparisons of semiclassical and quantum mechanical calculations for a variety of potential matrices. On the basis of the evidence so far accumulated, we conclude that for general three-dimensional two-state systems, Tully's fewest switches method is the most accurate semiclassical method currently available if (i) one uses the nonadiabatic coupling vector as the hopping vector and (ii) one propagates the trajectories in the representation that minimizes the number of surface hops.

## 1. Introduction

The radiationless decay of electronically excited molecules is a very important process in photoexcited systems.[1−5] It is widely appreciated that radiationless transitions are promoted by conical interactions and by the dynamical accessibility of low-energy pathways leading to such intersections.[6−8] In the present paper we consider the decay of a very simple electronically excited system, namely the $\tilde{A}\ ^2B_2$ state of $NaH_2$, and the effect of the accessibility of a conical intersection on its rate of decay and the accompanying internal conversion of electronic to vibrational−rotational−translational energy. In particular, we consider two different approximate potential energy matrices for this system, one[9] of which has a conical intersection near the minimum energy point of the $\tilde{A}\ ^2B_2$ surface, and the other[10] of which has a conical intersection that is 0.4 eV above the minimum energy point. Although the latter potential energy matrix is believed to be more accurate for this system, that is not the most important issue for the present study. Rather, we are interested in the effect that varying the potential energy matrix has on the observables calculated by semiclassical trajectory methods and on accurate quantal dynamics calculations. We ask, (1) What is the predicted effect of the variation in potential matrices on the lifetime and energy disposal? (2) Are the semiclassical predictions accurate for this effect? (3) Independent of their ability to predict the trends, how accurate are the semiclassical methods on an absolute basis for the radiationless decay lifetime and the amount of vibrational, rotational, and translational energy in the products?

We study two different semiclassical methods, trajectory surface hopping[11] and the Ehrenfest self-consistent-potential method;[12] the latter method is also called time-dependent self-consistent field theory. We compare the predictions of these semiclassical methods to accurate quantum results calculated by the outgoing wave variational principle. This study complements four earlier studies[13−16] of the accuracy (or inaccuracy) of these semiclassical methods. The first two studies[13,14] were concerned with electronic to vibrational−rotational energy transfer and bimolecular electronically nonadiabatic reactions in three-dimensional atom−diatom collisions. The first study[13] considered three systems involving conical intersections, including the $NaH_2$ system with the first of the potential energy matrices studied here. The second study[14] considered a system without a conical intersection in which the gap between the

* Corresponding author.
† University of Minnesota.
‡ NASA Ames Research Center.

10.1021/jp993353x CCC: $19.00 
Published on Web 12/16/1999

ground and excited electronic states is 0.46 eV or greater for all accessible geometries. The third study[15] was concerned with lifetimes and reactive branching ratios in unimolecular decay of a collinear triatomic system with an even larger gap, ~1 eV. The fourth study[16] considered the unimolecular decay of a three-dimensional triatomic system[10] with a conical intersection that is energetically inaccessible to many states in the exciplex well. The first potential energy matrix of ref 11 and the potential energy matrix of refs 10 and 16, both of which are approximations to the $NaH_2$ system, are the ones we consider in the present study. The current study extends the unimolecular decay calculations to a system with a conical intersection that is energetically accessible to all quasi-bound exciplex states, and it allows us to examine the dependence of the dynamical results on qualitative features of the potential energy matrices. The five studies (refs 13−16 and the present work) still do not span all qualitatively different varieties of systems with conical intersections, but they begin the process required to assemble a test set wide enough to question the generality of one's inferences. For example, if a semiclassical method underestimates the lifetimes for radiationless decay in a collinear system with a ~1 eV gap, does it show the same deficiency for three-dimensional systems with no gap?

Both the Ehrenfest method and Tully's fewest switches method have been applied to bound-state model systems[17] for which accurate quantum mechanical data were available. Both types of trajectory methods were found to agree qualitatively with the accurate quantum mechanical calculations. The system under investigation here differs from these model surfaces, however, in that the system is not fully bound (it can dissociate) and in that the ground and excited-state potential surfaces we consider have very different topologies from each other, as discussed in section 2. In particular, whereas the excited state has a potential energy well, the ground potential surface we consider is repulsive in every coordinate except the $H_2$ coordinate. The energy transfer process we consider is closer to the $O(^1D) + N_2(v,j) \rightarrow O(^3P) + N_2(v',j')$ reaction studied recently,[18] in which the ground state is bound but in which the excited state is repulsive. Surface hopping calculations were reported for the $NO_2$ system, but no accurate quantum dynamics were available for comparison.

A general criterion for the accuracy of nonadiabatic trajectory methods such as the Ehrenfest method and Tully's fewest switches method is that trajectories should follow similar paths on either potential surface in regions where the coupling is nonnegligible.[19] In the current work, this criterion is not satisfied, and it remains to be seen which, if either, of the two trajectory methods works best in this case. Another general criterion for the relative validity of the two semiclassical approaches is that self-consistent potential methods such as the Ehrenfest method work best for high-probability pathways and that trajectory methods work best for smaller-probability pathways.[20] One of the two potential matrices we investigate has small electronic couplings, while the other has a coupling that is much larger. In some sense then, the quenching products that we are examining are the dominant pathway for one potential matrix but represent a smaller-probability pathway for the other. This paper will test the Ehrenfest method and compare it to trajectory surface hopping for these cases.

A central issue in this paper, which has not been studied as much as it deserves, is a comparison of the relative accuracy of the adiabatic and diabatic representations for trajectory surface hopping calculations. In both representations the potential energy surfaces are given by the diagonal elements of the potential matrix. In the adiabatic approximation the potential matrix is diagonal, and the surfaces are coupled by the nuclear momentum (from the kinetic energy operator), whereas in the diabatic representation the potential matrix is nondiagonal and the coupling is provided by the off-diagonal potential. In an exact treatment there would also be momentum coupling in a diabatic representation, but the present paper is based on the invariant-space approximation[21] in which momentum coupling is zero in a diabatic representation.

We test three different criteria for predicting which representation is most accurate for trajectory surface hopping calculations. The first criterion requires trajectory surface hopping calculations in both representations. The second criterion that we test requires only the potential energy matrix and does not require any dynamical information. The third criterion requires accurate quantum mechanical results for both the fully coupled potential matrix and the uncoupled diabatic potential surfaces and uncoupled adiabatic potential surfaces. These three criteria will be presented in section 4.

Section 2 compares some characteristics of the potential energy matrices, such as energies and geometries at the asymptotes and the exciplex minimum and the seam of conical intersections. The semiclassical methods[11,12] under study are briefly summarized in section 3, along with the methods[22−24] used for accurate quantum calculations. Section 4 presents criteria for deciding which representation is best for surface hopping. Results are presented in section 5 and are discussed in section 6. Conclusions are summarized in section 7.

## 2. System

The process we consider is electronic predissociation, i.e., the unimolecular decay of an electronically excited-state complex to ground-electronic-state fragments, in particular

$$NaH_2(\kappa=2,v_1,v_2,v_3) \rightarrow Na(3s) + H_2(v',j') \qquad (1)$$

where the left-hand side describes an exciplex, $\kappa$ is the initial electronic state ($\kappa = 1$ is the electronic ground state, $\tilde{X}$, and $\kappa = 2$ is the first excited state, $\tilde{A}$, of $^2B_2$ symmetry for $C_{2v}$ geometries and $^2A'$ symmetry for $C_s$ geometries), $v_m$ ($m = 1$, 2, or 3) are the vibrational quantum numbers for the exciplex, and $v'$ and $j'$ are the final vibrational and rotational quantum numbers of $H_2$. The $\tilde{A}$ state corresponds formally to Na(3p) complexed to $H_2$, whereas the repulsive $\tilde{X}$ state corresponds to $Na(3s) + H_2$. Note that $v_1$ and $v_2$ are vibrations of $a_1$ symmetry, and $v_3$ is a vibration of $b_2$ symmetry. Thus, $v_1$ is an $H_2$ stretch (which may also be thought of as a symmetric stretch of H−Na−H), $v_2$ is a stretch of the coordinate from Na to $H_2$ (which may also be though of as a bend of H−Na−H), and $v_3$ is an angular motion in the Jacobi coordinate $\chi$ between the H−H axis and the Na-to-$H_2$ vector (which may also be thought of as an asymmetric stretch of H−Na−H). We consider only states with zero total angular momentum. In this work, we consistently neglect spin−orbit coupling and electronic angular momentum in both quantum and semiclassical dynamics calculations, and the form of the off-diagonal potential is chosen accordingly.[10]

We use two qualitatively different potential energy matrices for our calculations. The first potential energy matrix we consider is called potential matrix 5F.[9] The minimum potential energy point on the $\tilde{A}$ $^2B_2$ surface is located at an $H_2$ bond length of about 2.0 $a_0$. The depth of the well, $D_e$, relative to the Na(3p) + $H_2$ asymptote is 0.44 eV. Adding zero point energy yields a ground-state dissociation energy, $D_0$, of 0.48 eV. The conical intersection occurs very near the location of the minimum energy

**TABLE 1: Comparison of Potential Matrix 6 to Potential Matrix 5F[a]**

| | | potential matrix 5F | potential matrix 6 |
|---|---|---|---|
| minimum energy | $R_{Na-H_2}$ | 3.72 | 3.92 |
| point on the $\tilde{A}\ ^2B_2$ | $r_{H_2}$ | 1.98 | 1.50 |
| surface | $E$ | 1.667 (−0.437)[b] | 1.700 (−0.404)[b] |
| minimum energy | $R_{Na-H_2}$ | 3.70 | 3.59 |
| point of the conical | $r_{H_2}$ | 2.01 | 2.17 |
| intersection | $E$ | 1.668 (−0.436)[b] | 2.064 (−0.040)[b] |

[a] Zero of energy corresponds to Na infinitely far from $H_2$ on the $\tilde{X}\ ^2A_1$surface. All distances are in $a_0$; all energies are in eV. The Na excitation energy is 2.104 eV. [b] Values in parentheses are relative to the $\tilde{A}\ ^2B_2$ asymptote, whereas $E$ is relative to the $\tilde{X}\ ^2A_1$ asymptote.

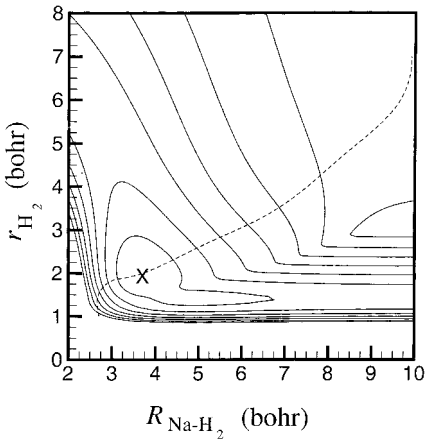


**Figure 1.** Potential energy contours of the upper diabatic surface in potential matrix 5F for $C_{2v}$ geometries. The contours shown are 2.0, 2.5, ..., 5.0 eV. The dashed line shows the line of conical intersections. The "X" shows the location of the lowest energy point on this surface.

point of the exciplex. The second potential energy matrix we consider is called potential matrix 6.[10] This potential matrix has $D_e = 0.40$ eV and $D_0 = 0.34$ eV. The minimum potential energy point on the $\tilde{A}\ ^2B_2$ surface of this potential matrix is located at values of the $H_2$ bond length only slightly larger than the equilibrium value of separated $H_2$. In this case, the conical intersection occurs at higher energies; the minimum energy along the conical intersection is roughly equal to the energy of the Na(3p) + $H_2$ asymptote. A more detailed comparison is provided in Table 1.

Contour plots of the upper diabatic surfaces of the two potential energy matrices are shown in Figures 1 and 2. In these figures and elsewhere in this paper, $R_{NaH_2}$ is the distance between Na and the center of mass of $H_2$ and $r_{H_2}$ is the $H_2$ bond length. It can be seen that the geometry of the equilibrium structure of the exciplex provides the single largest difference between the two diabatic surfaces. The location of the line of conical intersections is similar for both surfaces, but it occurs at higher energies for potential matrix 6 than for potential matrix 5F because of the difference in the geometry and shape of the exciplex.

The vibrational quantum numbers of each of the three exciplex modes, listed together, are used as a shorthand notation throughout this paper. For example, 000 refers to lowest energy exciplex state, and 100 refers to the state that has one quanta of energy in the $H_2$ vibrational mode.

## 3. Methods

**3.1. Quantum Dynamics.** We carried out accurate quantum scattering calculations in six dimensions (three vibrational internal coordinates and three rotational coordinates). Details

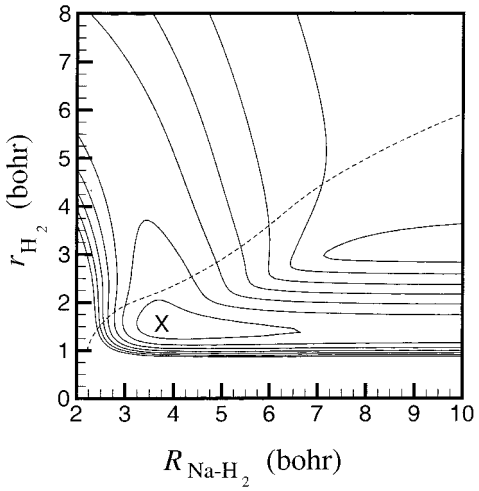


**Figure 2.** Potential energy contours of the upper diabatic surface in potential matrix 6 for $C_{2v}$ geometries. The dashed line shows the line of conical intersections. The "X" shows the location of the lowest energy point on this surface.

of the quantum mechanical scattering algorithm have been presented elsewhere.[22,23] Note that the fully coupled quantum mechanical results are independent of whether they are performed in an adiabatic or diabatic representation. (In general, one might expect differences due to approximations in the transformations or couplings; however, our coupled surfaces are both defined in the diabatic representation and—for the converged calculations—used in the diabatic representation, so there are no approximations, and the two representations are truly equivalent.)

We used the scattering calculations to locate and characterize predissociating states, which show up as Feshbach resonances.[24,25] A complete description of the procedure used to obtain the quantum mechanical observables has been presented recently,[16] and details have been presented in other places as well.[22,24]

We also performed variational bound-state calculations. Such calculations were performed for the uncoupled upper adiabatic and the upper diabatic potential energy surfaces of $NaH_2$ potential matrix 5F and of $NaH_2$ potential matrix 6. These calculations included all potential energy couplings between the nuclear coordinates, and they used the exact kinetic energy operator. The program used is described elsewhere.[26]

**3.2. Semiclassical Methods.** The semiclassical trajectory methods considered here are both trajectory-based methods including the full dimensionality of the system. In particular, we consider Tully's fewest switches[11] (TFS) version of trajectory surface hopping, and we consider the Ehrenfest self-consistent potential[12] (ESCP) method. The latter is also called the time-dependent self-consistent field (TDSCF) method. In this section we review the essentials of both kinds of methods and compare them.

Since motion of the overall center of mass is irrelevant, all trajectories are six-dimensional. In both of the semiclassical trajectory methods that we consider, a distinction is made between quantum variables, **r**, and classical variables, **R**, where **R** is the six-dimensional vector of nuclear coordinates. The classical variables are assumed to be described by an ensemble of trajectories $\mathbf{R}(t)$, and the time-dependent Schrödinger equation is written

$$H_{el}(\mathbf{r};\mathbf{R}(t))\ \Phi(\mathbf{R}(t);\mathbf{r}) = i\hbar\frac{\partial}{\partial t}\Phi(\mathbf{R}(t);\mathbf{r}) \qquad (2)$$

where $H_{el}$ is the electronic Hamiltonian and $\Phi$ is the wave function for the quantum variable **r** and depends on $t$ through the trajectory $\mathbf{R}(t)$. The electronic wave function $\Phi$ is expanded in terms of basis functions $\{\phi_j\}$:

$$\Phi(\mathbf{R}(t);\mathbf{r}) = c_1(t)\,\eta_1(t)\,\phi_1(\mathbf{r};\mathbf{R}(t)) + c_2(t)\,\eta_2(t)\,\phi_2(\mathbf{r};\mathbf{R}(t)) \tag{3}$$

where the coefficients $\{c_j\}$ are complex, the phase factors $\eta_1(t)$ and $\eta_2(t)$ are given by

$$\eta_i(t) = \exp\left(-\frac{\mathrm{i}}{\hbar}\int^t V_{ii}(\mathbf{R}(t))\,\mathrm{d}t\right) \tag{4}$$

and

$$V_{kj}(\mathbf{R}) = \langle\phi_k(\mathbf{r};\mathbf{R})|H_{el}(\mathbf{r};\mathbf{R}(t))|\phi_j(r;R)\rangle \tag{5}$$

and we have limited our discussion to two-state systems. Equation 5 defines a potential energy matrix. Substituting eq 3 into eq 2, multiplying from the left by $\phi_1$ or $\phi_2$, and integrating give

$$\dot{c}_1(t) = -c_2(t)\left[\frac{\mathrm{i}}{\hbar}V_{12}(\mathbf{R}(t)) + \dot{\mathbf{R}}\cdot\mathbf{d}_{12}(\mathbf{R}(t))\right]\frac{\eta_1(t)}{\eta_2(t)} \tag{6}$$

and

$$\dot{c}_2(t) = c_1(t)\left[\frac{\mathrm{i}}{\hbar}V_{21}(\mathbf{R}(t)) + \dot{\mathbf{R}}\cdot\mathbf{d}_{21}(\mathbf{R}(t))\right]\frac{\eta_2(t)}{\eta_1(t)} \tag{7}$$

where

$$\mathbf{d}_{kj}(\mathbf{R}) = \langle\phi_k(\mathbf{r};\mathbf{R})|\nabla_{\mathbf{R}}\phi_j(\mathbf{r};\mathbf{R})\rangle \tag{8}$$

and $\nabla_{\mathbf{R}}$ is the gradient with respect to the nuclear coordinates. Note that adiabatic basis functions are only coupled by off-diagonal derivative matrix elements, defined in eq 8, while true diabatic basis functions would only be coupled by off-diagonal potential matrix elements. The calculation of the **d** matrix from the potentials defined in eq 8 was described previously.[16]

Equations 6 and 7 describe the evolution of the electronic wave function $\Phi$ along a trajectory $\mathbf{R}(t)$. The coefficients $c_1(t)$ and $c_2(t)$ are the probability amplitudes for finding the system in state $\phi_1$ or $\phi_2$, respectively, if a measurement is made at time $t$. In both the TFS and ESCP methods, the system is assumed to be described by an ensemble of trajectories generated by averaging over quasiclassical[27,28] initial conditions. Both methods make the independent trajectory assumption; i.e., the trajectories constituting the ensemble are decoupled from one another. The essential difference between the ESCP method and trajectory surface hopping methods such as the TFS method is the way in which the trajectory $\mathbf{R}(t)$ depends on the quantal wave function $\Phi$.

In the ESCP method, the trajectory $\mathbf{R}(t)$ is propagated on a potential energy surface given by

$$V(\mathbf{R}) = \langle\Phi(\mathbf{r};\mathbf{R})|H_{el}(\mathbf{r};\mathbf{R})|\Phi(\mathbf{r};\mathbf{R})\rangle \tag{9}$$

Thus, as the basis function coefficients evolve with time, the potential changes accordingly. If either $c_1(t)$ or $c_2(t)$ is equal to zero, then the potential energy given by eq 9 is identical to one of the diagonal potential energy matrix elements. In general, however, the potential energy experienced by an Ehrenfest trajectory will include contributions from the diagonal and off-diagonal matrix elements. The meaning and physicality of this surface have been discussed elsewhere.[11,29]

In the TFS method, trajectories are propagated on the diagonal potential matrix elements. The number of trajectories that propagate on a given surface is proportional to the probability for finding the system in state $\phi_1$ or state $\phi_2$. As the probabilities change over time, the correct surface populations are maintained by allowing some trajectories to switch surfaces. The hopping scheme in which the smallest number of trajectories switch surfaces over a time interval while satisfying the constraint that the correct surface populations be maintained is called Tully's fewest switches algorithm.[11]

A critical element in trajectory surface hopping calculations is the choice of hopping vector, which is a unit vector along whose direction the nuclear momentum is incremented or decremented whenever a hop occurs. In this paper, we performed the TFS calculations with two different hopping vectors. These vectors have been described in a recent paper,[16] they are the nonadiabatic coupling vector (**d**)[30,31] and the rotated **d** vector.[16] In that work we discussed the use of two additional vectors, the gradient of the difference of the adiabatic energy (**g**)[32,33] and the rotated **g** vector.[16] We found, using potential matrix 6, that the **d** vector calculations agreed with the accurate quantum calculations better than the **g** vector calculations did both in the trends of final product distributions as functions of the energy and in the absolute errors of the final product distributions. We also mention that earlier calculations for potential matrix 5F showed no notable difference between the **g** and the **d** vectors.[13] For these reasons, we omit calculations with the **g** and rotated **g** vectors in the present work, and we present results for the **d** and rotated **d** vectors only.

Traditionally, trajectory surface hopping calculations are carried out in the adiabatic representation, but in this study we performed the TFS calculations in both the diabatic and the adiabatic representations. We note that use of the nonadiabatic coupling vector **d** may seem more natural for calculations in the adiabatic representation, but it may be calculated uniquely from diabatic information,[16] and there is no inconsistency in using it for the hopping vector in either representation. Whereas the surface hopping calculations depend on the choice of electronic representation (adiabatic or diabatic), the ESCP method is invariant to this choice.[12]

In all of our TFS calculations, we employ the adaptive numerical integration scheme discussed in a recent paper[16] to ensure that our TFS calculations are adequately converged with respect to the integration step size.

The methods used for final state analysis have been described elsewhere,[13,16] and so we only briefly review them here. In the histogram method,[13,28] the final continuous classical quantities (such as the vibrational and rotational quantum numbers) are rounded to the nearest discrete quantum mechanical values. In the linear smooth sampling (LSS)[13,28,34−36] and quadratic smooth sampling (QSS)[13,37] methods, the classical quantity contributes to the two nearest quantum numbers that bracket it. In the LSS method the farther quantum number is weighted by the distance of the classical value from the nearest quantum number, and the nearest quantum number is weighted by the distance of the classical value from the farther quantum number. In the QSS method, the weight of the farther quantum number is given by the square of the distance of the classical value from the nearest quantum number, and the weight of the nearest quantum number is chosen such that the two weights sum to unity (in the case where the quantum numbers are restricted to even or odd values, the weights in both the LSS and QSS methods are appropriately

normalized). Note that in the Ehrenfest method the electronic quantum number is in general noninteger and must be assigned according to one of these three schemes along with the rotational and vibrational quantum numbers. Probably for this reason, the results of the Ehrenfest method depend significantly on whether histograming, LSS, or QSS is used to analyze the final state. The TFS methods, on the other hand, give very similar results with all three analysis methods for the present system. Therefore, we present only the histogram results for the TFS methods, and we present results from all these methods for the Ehrenfest calculations.

Analytical derivatives for $NaH_2$ potential matrix 6 were calculated using the ADIFOR[38] program, while analytical derivatives for $NaH_2$ potential matrix 5F were derived by hand.

### 4. Criteria for Surface Hopping

We consider three possible criteria for deciding which representation is best for surface hopping calculations.

**4.1. Hop Minimization.** Our first criterion for which representation should be used for the surface hopping calculations is that it is the representation that leads to the smallest number of surface hops. This criterion has been suggested by Tully.[39] We label the representation in which the fewest number of surface hops occurs "hm" or the hop-minimizing representation.

**4.2. Volume of Surface Coupling.** We calculated the nonadiabatic coupling and the diabatic coupling at a wide range of geometries in order to compare the two potential matrices to one another. In particular, we define the following phase space volumes for each potential matrix:

$$W_{\mathrm{dia}}(E) = \int_{\mathbf{R}}\int_{\mathbf{P}} \mathrm{d}^{3N-3}\mathbf{R}\, \mathrm{d}^{3N-3}\mathbf{P} \left[\frac{V_{21}(\mathbf{R})}{\hbar}\right] \qquad (10)$$

and

$$W_{\mathrm{adi}}(E) = \int_{\mathbf{R}}\int_{\mathbf{P}} \mathrm{d}^{3N-3}\mathbf{R}\, \mathrm{d}^{3N-3}\mathbf{P}\, [\mathbf{v}(\mathbf{P})\cdot\mathbf{d}_{21}(\mathbf{R})] \qquad (11)$$

where $E$ is the total energy, $V_{21}(\mathbf{R})$ is derived from eq 5 by using diabatic basis functions, $\mathbf{d}_{21}(\mathbf{R})$ is derived from eq 8 by using adiabatic basis functions, $\mathbf{P}$ is the 6-dimensional nuclear momentum, and $\mathbf{v}$ is the 6-dimensional nuclear velocity. In eq 10 we integrate over all phase points where the upper diabatic potential energy surface is energetically accessible, and in eq 11 we integrate over all phase points where the upper adiabatic potential surface is energetically accessible. The motivation for limiting the integration to these regions of phase space is that classical transitions between potential surfaces can only occur in these regions. Additional constraints on the integrals in eqs 10 and 11 are that for a particular $\mathbf{R}$ and $\mathbf{P}$, the total energy $E$ must be conserved. We define

$$^1/_2P^2 = T = E - V_{\mathrm{av}}(\mathbf{R}) \qquad (12)$$

where

$$V_{\mathrm{av}}(\mathbf{R}) = {}^1/_2(V_{11}(\mathbf{R}) + V_{22}(\mathbf{R})) \qquad (13)$$

Finally, we require that the total angular momentum be zero. Further details about these calculations are provided in Appendix A.

Our second criterion for the selection of the representation for the trajectory surface hopping calculations is that they should be performed in the representation that has the smallest volume of coupling.

Note that we have not included the energy gap between potential surfaces in eqs 10 and 11, as might be expected from a first-order time-dependent perturbation treatment of the coupled equations (6) and (7). One of the approximations typically invoked in such a treatment[40] is that the energy gap between unperturbed states is constant with time. In our case, where the ground-state potential energy surface has a very different topology from the excited-state potential energy surface, this approximation is invalid. It is especially poor near crossings of the potential surfaces, which occur along a one-dimensional seam in the adiabatic representation and which occur along a two-dimensional surface in the diabatic representation. This illustrates a second problem with including such an energy gap term in our integrals, namely that the two representations are no longer treated equivalently. This is because the approximation is worse for the diabatic representation than for the adiabatic representation due to the larger dimensionality of the surface crossing for the diabatic case.

Tully has shown[11] that the rates of change in the electronic probabilities for a two-state system are given by

$$\dot{P}_1 = 2\mathrm{Im}[a_{12}^*(t)]\frac{V_{12}(\mathbf{R}(t))}{\hbar} - 2\mathrm{Re}[a_{12}^*(t)]\dot{\mathbf{R}}\cdot\mathbf{d}_{12}(\mathbf{R}(t)) \qquad (14)$$

$$\dot{P}_2(t) = -\dot{P}_1(t) \qquad (15)$$

where

$$a_{12}^*(t) = c_1^*(t)\, \eta_1^*(t)\, c_2(t)\, \eta_2(t) \qquad (16)$$

Note that the electronic coherence $a_{12}^*(t)$ contributes to the rate that the probabilities change with time, but the coherence is not a local property of the potential matrix. A first-order time-dependent perturbation theory treatment of eq 14 reveals that the electronic coherence depends on the potential energy gap and that only by assuming the energy gap is constant with time can this gap be factored out of the resulting time integral. The only accurate way to treat the electronic coherence is to integrate it over time, i.e., to calculate a trajectory. We may still obtain insight into the nature of the coupling without calculating trajectories, however, by simply neglecting the coherence terms altogether and considering the quantities $V_{21}(\mathbf{R})$ and $\dot{\mathbf{R}}\cdot\mathbf{d}_{12}(\mathbf{R})$ as the only sources of coupling, as we have done in eqs 10 and 11. The drawback from this procedure is that the coupling at large-gap regions of phase space contributes to the integrals (10) and (11) with as much weight as the coupling at small-gap regions of phase space does.

**4.3. Quantum Mechanical Calculations.** Taken together, the single-surface bound-state calculations and the fully coupled quantum mechanical calculations allow us to determine which representation provides a better uncoupled model of the system. In particular, we compare the single-surface bound-state energies for both the upper adiabatic potential energy surface and the upper diabatic potential energy surface to the energies of the quantum mechanical resonances as determined from the fully coupled calculations. Our third criterion for the selection of the representation for the trajectory surface hopping calculations is that the representation of the single-surface bound-state calculation that best agrees with the fully coupled calculations should be used for the surface hopping calculations.

**TABLE 2: Comparison of Bound-State Quantum Mechanical Calculations and Fully Coupled Quantum Mechanical Calculations for Potential Energy Matrix 5F[a]**

| | | fully coupled | | | | | adiabatic bound state | | diabatic bound state | |
|---|---|---|---|---|---|---|---|---|---|---|
| α | state[b] | $E_\alpha$ | $E_\alpha - E_0$ | $\Gamma_\alpha$ | $\langle v' \rangle$ | $\langle j' \rangle$ | $E_\alpha$ | $E_\alpha - E_0$ | $E_\alpha$ | $E_\alpha - E_0$ |
| 0 | 000 | 1.890 | 0.000 | 1.960 | 1.64 | 1.36 | 1.944 | 0.000 | 1.881 | 0.000 |
| 1 | 010 | 1.977 | 0.087 | 4.697 | 1.92 | 2.02 | 2.030 | 0.086 | 1.968 | 0.088 |
| 2 | 020 | 2.053 | 0.163 | 5.741 | 2.17 | 2.49 | 2.119 | 0.175 | 2.047 | 0.166 |
| 3 | 002 | 2.080 | 0.190 | wide | | | 2.085 | 0.141 | 2.069 | 0.188 |
| 4 | 100 | 2.105 | 0.215 | 2.474 | 2.14 | 2.83 | 2.240 | 0.296 | 2.007 | 0.216 |

[a] Energies ($E_\alpha$ and $E_\alpha - E_0$) are in eV, and widths ($\Gamma_\alpha$) are in meV. α labels the resonance, and $E_\alpha$ is the energy of resonance α. [b] Vibrational quantum numbers $v_1$, $v_2$, and $v_3$ as defined in section 2.

**TABLE 3: Comparison of Bound-State Quantum Mechanical Calculations and Fully Coupled Quantum Mechanical Calculations for Potential Energy Matrix 6[a]**

| | | fully coupled | | | | | adiabatic bound state | | diabatic bound state | |
|---|---|---|---|---|---|---|---|---|---|---|
| α | state[b] | $E_\alpha$ | $E_\alpha - E_0$ | $\Gamma_\alpha$ | $\langle v' \rangle$ | $\langle j' \rangle$ | $E_\alpha$ | $E_\alpha - E_0$ | $E_\alpha$ | $E_\alpha - E_0$ |
| 0 | 000 | 2.030 | 0.000 | 1.442 | 0.82 | 8.34 | 2.030 | 0.000 | 2.024 | 0.000 |
| 1 | 010 | 2.093 | 0.063 | 1.279 | 0.74 | 7.69 | 2.094 | 0.064 | 2.087 | 0.063 |
| 2 | 020 | 2.147 | 0.117 | 1.385 | 0.84 | 7.25 | 2.148 | 0.118 | 2.141 | 0.117 |
| 3 | 001 | 2.184 | 0.154 | 0.608 | 1.85 | 5.67 | 2.184 | 0.154 | 2.170 | 0.146 |
| 4 | 030 | 2.193 | 0.163 | 1.222 | 1.09 | 5.67 | 2.194 | 0.164 | 2.188 | 0.164 |
| 5 | 040 | 2.232 | 0.202 | 1.116 | 1.20 | 4.85 | 2.233 | 0.203 | 2.229 | 0.205 |
| 6 | 050 | 2.267 | 0.237 | 1.020 | 1.30 | 4.32 | 2.268 | 0.238 | 2.264 | 0.240 |
| 7 | 002 | 2.273 | 0.243 | 0.522 | 1.35 | 8.82 | 2.273 | 0.243 | 2.259 | 0.235 |
| 8 | 060 | 2.296 | 0.266 | 0.848 | 1.34 | 3.73 | 2.297 | 0.267 | 2.291 | 0.267 |
| 9 | 100 | 2.302 | 0.272 | 2.871 | 2.41 | 2.98 | 2.304 | 0.274 | 2.294 | 0.270 |

[a] Energies ($E_\alpha$ and $E_\alpha - E_0$) are in eV, and widths ($\Gamma_\alpha$) are in meV. α labels the resonance, and $E_\alpha$ is the energy of resonance α. [b] Vibrational quantum numbers $v_1$, $v_2$, and $v_3$.

## 5. Results

Tables 2 and 3 show the energies and widths of the quantum mechanical resonances, the energies of bound states in the adiabatic approximation, and the energies of bound states in the diabatic approximation for each potential energy matrix.

In all figures, we use the following notation for the TSH methods: solid lines represent adiabatic calculations, and dashed lines represent diabatic calculations; open squares represent the rotated TFS-**d** method, and filled squares represent the nonrotated TFS-**d** method. The Ehrenfest method is shown with circles linked by solid lines. Open circles represent Ehrenfest trajectories analyzed with histogram methods, black circles represent Ehrenfest trajectories analyzed with linear smooth sampling, and circles with plus signs inside represent Ehrenfest trajectories analyzed with quadratic smooth sampling. Quantum mechanical results are indicated with thick black lines.

We use the following notation for clarity in discussing the four TFS methods. The vector used for hopping is indicated after the "TFS" abbreviation in bold. Rotation is indicated by "rot" before the hopping vector, and nonrotated methods are indicated by "nr". Adiabatic methods are labeled with "adiabatic" preceding the abbreviation, and diabatic methods are labeled with "diabatic" preceding the abbreviation. Thus, diabatic-TFS-rot-**d** refers to the diabatic rotated-**d** TFS method, while adiabatic-TFS-nr-**d** refers to the adiabatic nonrotated-**d** TFS method. When a method is mentioned without such a label, the reference is assumed to apply to all variants of that method, independent of the missing label. For example, diabatic-TFS-**d** refers to both rotated and nonrotated methods, and TFS-nr-**d** refers to both adiabatic and diabatic representations of the nonrotated-**d** TFS method.

The notation used for the ESCP method is Ehrenfest-Hist, Ehrenfest-LSS, and Ehrenfest-QSS for the histogrammed Ehrenfest results, the linear smooth sampling Ehrenfest results, and the quadratic smooth sampling Ehrenfest results, respectively.

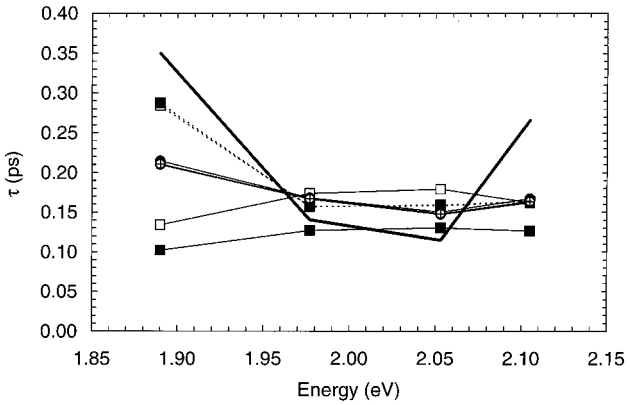


**Figure 3.** Mean decay lifetime versus total energy for the resonances of potential matrix 5F. Solid squares represent TFS-nr-**d** methods, and open squares represent TFS-rot-**d** methods; solid lines represent calculations employing the adiabatic representation, and dotted lines represent calculations employing the diabatic representation. The circles represent Ehrenfest calculations. The degree of filling of the circles indicates the method used to analyze the Ehrenfest method: black indicates LSS, pluses indicate QSS, and no filling indicates histogramming. The thick black line with no symbols indicates the converged quantum mechanics calculations, which are independent of the choice of electronic representation.

Figures 3−6 show plots of the lifetime, the average final vibrational quantum number, the average final rotational quantum number, and the average final relative translational energy for semiclassical trajectory calculations for $NaH_2$ potential energy matrix 5F. Figures 7−10 show plots of the same quantities for semiclassical trajectory calculations on $NaH_2$ potential energy matrix 6; in these plots, we present the trajectories in three groups, according to which mode is excited. We include the 000 resonance in each of the three groups, to make clear the trends of the quantities with energy and quantum numbers. Average overall errors are shown in Tables 4 and 5 for each potential energy matrix.

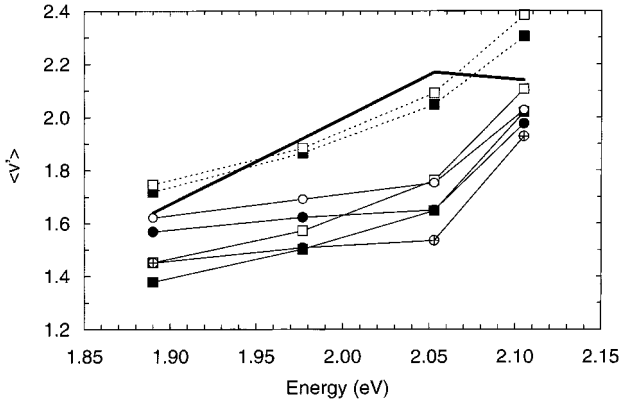


**Figure 4.** Average final vibrational quantum number versus the total energy for resonances for potential matrix 5F. Solid squares represent TFS-nr-**d** methods, and open squares represent TFS-rot-**d** methods; solid lines represent calculations employing the adiabatic representation, and dotted lines represent calculations employing the diabatic representation. The circles represent Ehrenfest calculations. The degree of filling of the circles indicates the method used to analyze the Ehrenfest method: black indicates LSS, pluses indicate QSS, and no filling indicates histogramming. The thick black line with no symbols indicates the converged quantum mechanics calculations, which are independent of the choice of electronic representation.

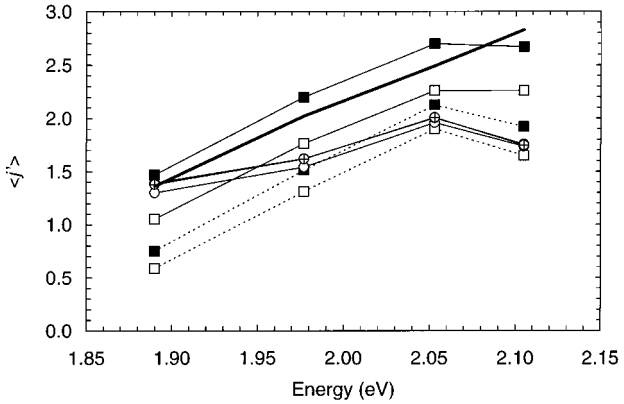


**Figure 5.** Average final rotational quantum number versus the total energy for resonances for potential matrix 5F. Solid squares represent TFS-nr-**d** methods, and open squares represent TFS-rot-**d** methods; solid lines represent calculations employing the adiabatic representation, and dotted lines represent calculations employing the diabatic representation. The circles represent Ehrenfest calculations. The degree of filling of the circles indicates the method used to analyze the Ehrenfest method: black indicates LSS, pluses indicate QSS, and no filling indicates histogramming. The thick black line with no symbols indicates the converged quantum mechanics calculations, which are independent of the choice of electronic representation.

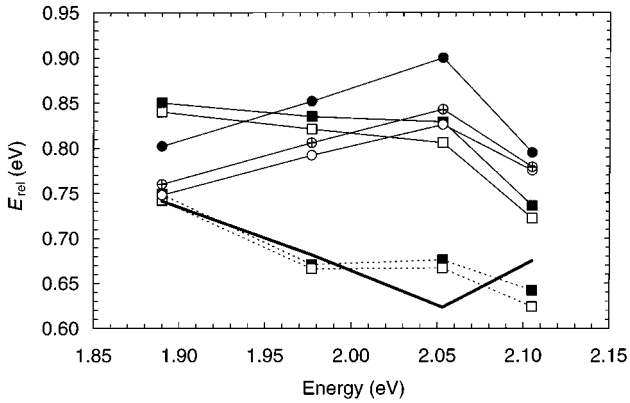


**Figure 6.** Final relative energy versus the total energy for resonances for potential matrix 5F. Solid squares represent TFS-nr-**d** methods, and open squares represent TFS-rot-**d** methods; solid lines represent calculations employing the adiabatic representation, and dotted lines represent calculations employing the diabatic representation. The circles represent Ehrenfest calculations. The degree of filling of the circles indicates the method used to analyze the Ehrenfest method: black indicates LSS, pluses indicate QSS, and no filling indicates histogramming. The thick black line with no symbols indicates the converged quantum mechanics calculations, which are independent of the choice of electronic representation.

**TABLE 4: Semiclassical RMS Errors in the Mean Lifetime, in the Final Average Vibrational Quantum Number, in the Final Average Rotational Quantum Number, and in the Average Final Relative Energy for Potential Matrix 5F[a]**

Absolute RMS Errors

| | nr-**d** | | rot-**d** | | Ehrenfest | | |
|---|---|---|---|---|---|---|---|
| | ad-TFS[b] | di-TFS[c] | ad-TFS[b] | di-TFS[c] | Hist | LSS | QSS |
| $\tau$ (ps) | 0.14 | **0.04** | 0.11 | **0.04** | 0.07 | 0.09 | 0.09 |
| $\langle v' \rangle$ | 0.36 | **0.11** | 0.28 | 0.14 | 0.24 | 0.31 | 0.40 |
| $\langle j' \rangle$ | **0.17** | 0.63 | 0.37 | 0.84 | 0.66 | 0.62 | 0.63 |
| $\langle E_{rel} \rangle$ (eV) | 0.14 | **0.03** | 0.13 | **0.03** | 0.13 | 0.18 | 0.14 |

Relative RMS Errors (%)

| | nr-**d** | | rot-**d** | | Ehrenfest | | |
|---|---|---|---|---|---|---|---|
| | ad-TFS[b] | di-TFS[c] | ad-TFS[b] | di-TFS[c] | Hist | LSS | QSS |
| $\tau$ (ps) | 45 | **29** | 48 | **29** | 33 | 33 | 33 |
| $\langle v' \rangle$ | 18 | **6** | 14 | 7 | 12 | 15 | 20 |
| $\langle j' \rangle$ | **8** | 31 | 17 | 41 | 25 | 24 | 24 |
| $\langle E_{rel} \rangle$ (eV) | 22 | **5** | 19 | **5** | 20 | 27 | 21 |

[a] Bold numbers indicate the lowest error for each of the four quantities. [b] Adiabatic Tully's fewest switches algorithm. [c] Diabatic Tully's fewest switches algorithm.

We gathered statistics on the surface hops of the TFS calculations. In particular, for each method and for each potential matrix, we calculated the number of successful surface hops, the number of hops that failed due to insufficient energy, and the number of hops that failed due to insufficient linear momentum along the hopping vector. Note that the rotated vector methods have no linear momentum prohibited hops. It is possible for a rotated vector method to have angular momentum prohibited hops.[16] These occur when there is sufficient kinetic energy to hop, but a large portion of the energy is contained in rotational motion of the system as a whole. In this case angular momentum conservation limits the momentum adjustment that is allowed. If the energy associated with the internal vibrational motion of the system is smaller than the potential energy gap, then hops are not allowed. For nonrotated vector methods, this class of hopping failure falls into the more general case of momentum prohibited hops. In our present calculations, the total angular momentum is extremely small, and we observed no angular momentum prohibited hops. Table 6 shows the hopping statistics. According to our first criterion, semiclassical trajectory surface hopping should be performed in the representation in which the fewest number of hops occurs. From Table 6 it is apparent that for potential matrix 5F, the hop-minimizing (hm) representation is the diabatic representation, and for potential matrix 6 it is the adiabatic representation.

In addition to looking at the number of successful and attempted hops, we looked at average potential energy changes during hopping, as well as the kinetic energy prior to hopping. Figure 11 shows a plot of the average potential energy change for both potential matrices, and Figure 12 shows ratios of the average kinetic energy to the average potential energy gap for each potential matrix.

Figure 13 shows a plot of the volume of diabatic and nonadiabatic coupling for each potential matrix as a function

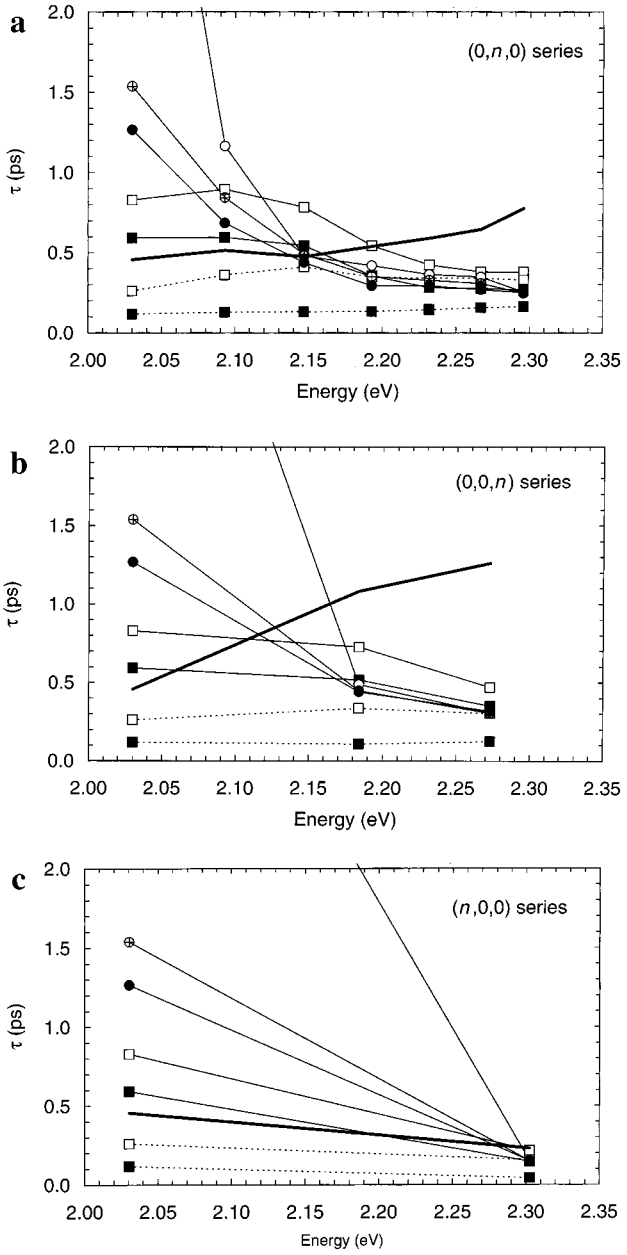


**Figure 7.** Decay lifetimes versus total energy for resonances for potential matrix 6: (a) 0*n*0 series; (b) 00*n* series; (c) *n*00 series. Solid squares represent TFS-nr-**d** methods, and open squares represent TFS-rot-**d** methods; solid lines represent adiabatic calculations, and dotted lines represent diabatic calculations. The circles represent Ehrenfest calculations. The degree of filling of the circles indicates the method used to analyze the Ehrenfest method: black indicates LSS, pluses indicate QSS, and no filling indicates histogramming. The thick black line with no symbols indicates the quantum mechanics calculations.

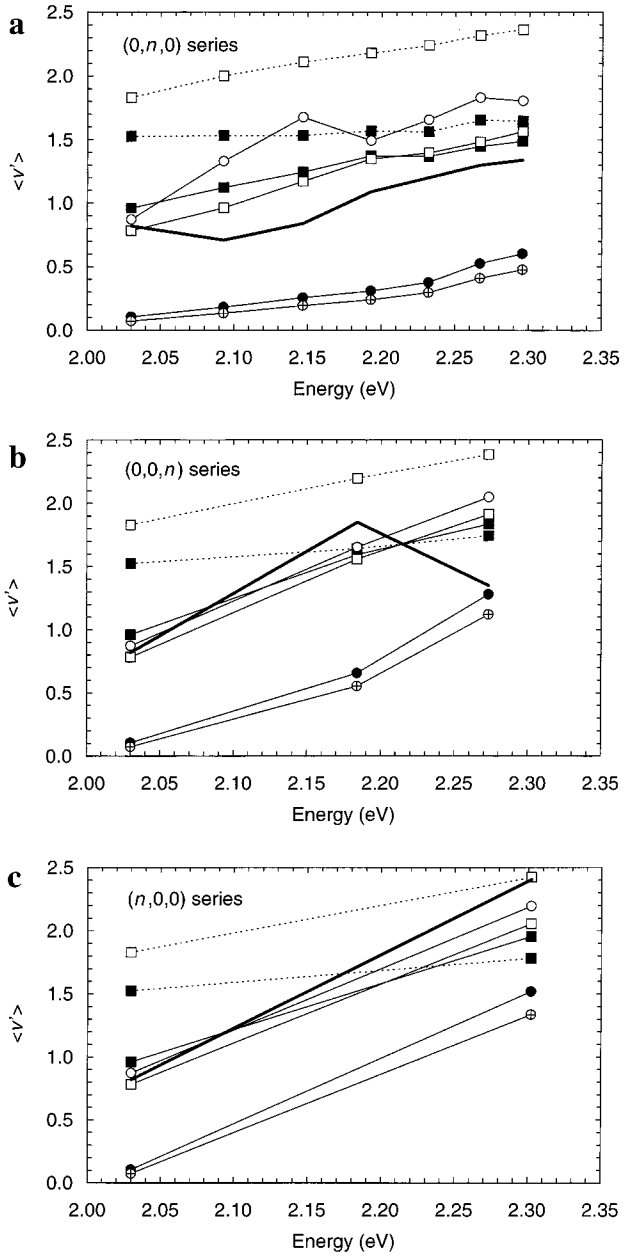


**Figure 8.** Final average vibrational quantum number versus the total energy for resonances for potential matrix 6: (a) 0*n*0 series; (b) 00*n* series; (c) *n*00 series. Solid squares represent TFS-nr-**d** methods, and open squares represent TFS-rot-**d** methods; solid lines represent adiabatic calculations, and dotted lines represent diabatic calculations. The circles represent Ehrenfest calculations. The degree of filling of the circles indicates the method used to analyze the Ehrenfest method: black indicates LSS, pluses indicate QSS, and no filling indicates histogramming. The thick black line with no symbols indicates the quantum mechanics calculations.

of energy. For potential matrix 5F, the diabatic coupling volume is much larger than the nonadiabatic coupling volume. For potential matrix 6, the opposite is true. Our second criterion suggests that the diabatic representation should be used for trajectory surface hopping calculations for potential matrix 5F and that the adiabatic representation should be used for potential matrix 6.

## 6. Discussion

**6.1. Comparison of Quantum Mechanical Calculations for Potential Matrix 5F and Potential Matrix 6.** We compare six quantities between the quantum mechanical calculations for potential matrix 5F and those for potential matrix 6. The six trends to be compared are the spacings of the resonance levels, the lifetimes of the resonances, the average vibrational quantum number of the decay products, the average rotational number of the decay products, the average translational energy of the products, and the superiority of a particular electronic representation in the single-surface bound-state calculations.

For both potential matrices, the energy spacings of the resonances are closely related to the shape of the exciplex potential energy well. For example, the zero point energy and 100 resonance energy of the exciplex for potential matrix 6 are slightly larger than they are for potential matrix 5F. This is

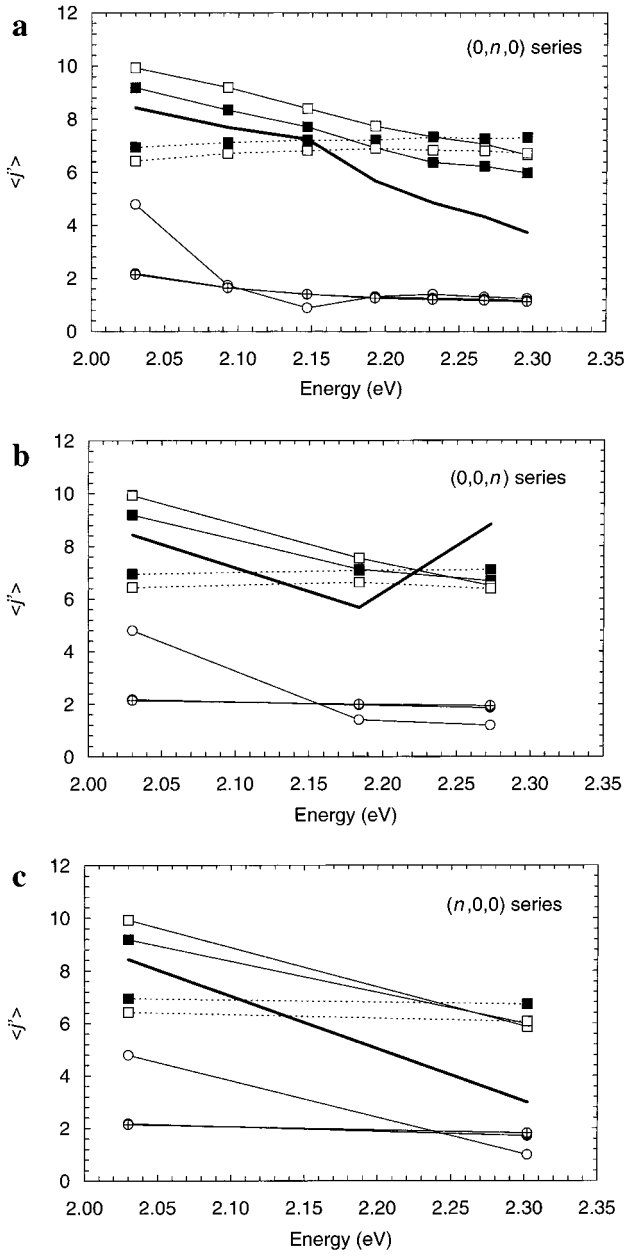


**Figure 9.** Final average rotational quantum number versus the total energy for resonances for potential matrix 6: (a) 0*n*0 series; (b) 00*n* series; (c) *n*00 series. Solid squares represent TFS-nr-**d** methods, and open squares represent TFS-rot-**d** methods; solid lines represent adiabatic calculations, and dotted lines represent diabatic calculations. The circles represent Ehrenfest calculations. The degree of filling of the circles indicates the method used to analyze the Ehrenfest method: black indicates LSS, pluses indicate QSS, and no filling indicates histogramming. The thick black line with no symbols indicates the quantum mechanics calculations.

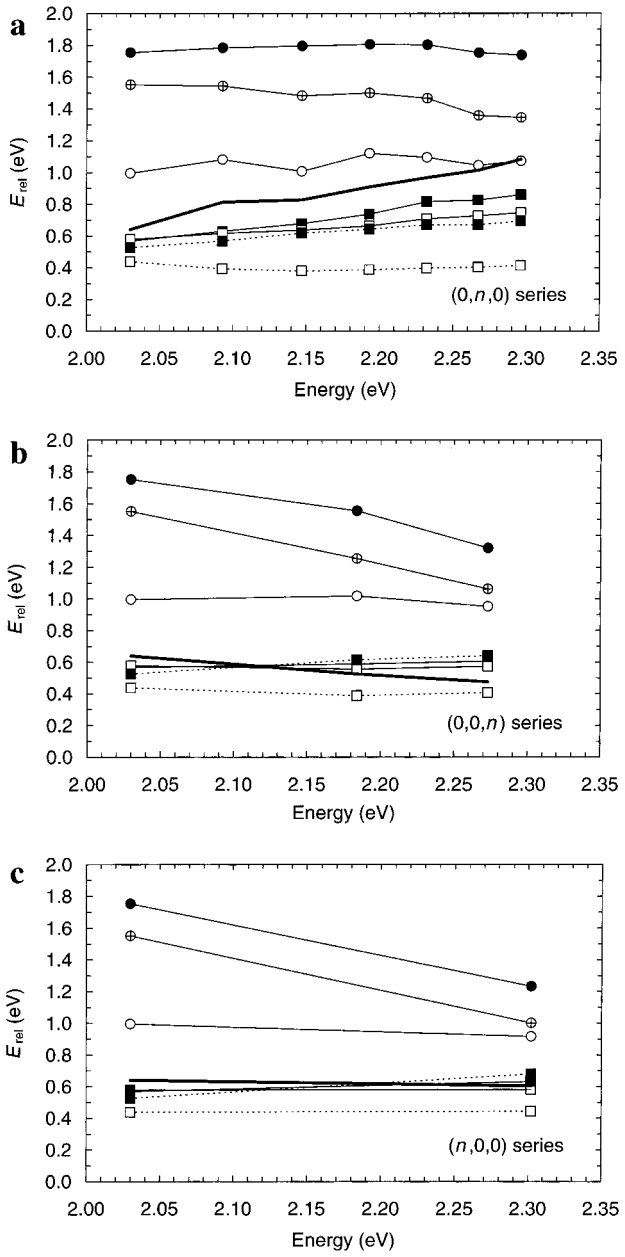


**Figure 10.** Final relative energy versus the total energy for resonances for potential matrix 6: (a) 0*n*0 series; (b) 00*n* series; (c) *n*00 series. Solid squares represent TFS-nr-**d** methods, and open squares represent TFS-rot-**d** methods; solid lines represent adiabatic calculations, and dotted lines represent diabatic calculations. The circles represent Ehrenfest calculations. The degree of filling of the circles indicates the method used to analyze the Ehrenfest method: black indicates LSS, pluses indicate QSS, and no filling indicates histogramming. The thick black line with no symbols indicates the quantum mechanics calculations.

consistent with the shape of the well for potential matrix 6, which is narrower in the $r_{H_2}$ direction than that for potential matrix 5F. This is shown in Figures 1 and 2. On the other hand, it can be seen that the energies of the 010 and 020 states for potential matrix 5F are slightly higher than those for potential matrix 6. This again is consistent with the geometry of the well for potential matrix 6, which is wider in the $R_{NaH_2}$ coordinate than it is for potential matrix 5F, as shown in Figures 1 and 2.

The total resonance widths tend to be larger for potential matrix 5F than they are for potential matrix 6, indicating that the exciplexes for potential matrix 5F have shorter lifetimes than they do for potential matrix 6. This also indicates that the electronic states for potential matrix 5F are more strongly coupled than the electronic states for potential matrix 6. This is correlated with the relative magnitudes of the diabatic and nonadiabatic coupling for each potential matrix. The nonadiabatic coupling is strongest near the line of conical intersections. For potential matrix 5F, the conical intersection passes close to the bottom of the exciplex, where the vibrational wave function density is highest. For potential matrix 6 the conical intersection passes farther from the bottom of the well, where the vibrational wave function density is lower. The nonadiabatic coupling will thus more strongly couple the states in potential matrix 5F than the states in potential matrix 6. For both potential matrices the

**TABLE 5: Semiclassical RMS Errors in the Mean Lifetime, in the Final Average Vibrational Quantum Number, in the Final Average Rotational Quantum Number, and in the Average Final Relative Energy for Potential Matrix 6[a]**

| Absolute RMS Errors | | | | | | | |
|---|---|---|---|---|---|---|---|
| | nr-**d** | | rot-**d** | | Ehrenfest | | |
| | ad-TFS[b] | di-TFS[c] | ad-TFS[b] | di-TFS[c] | Hist | LSS | QSS |
| $\tau$ (ps) | 0.41 | 0.60 | **0.37** | 0.44 | 1.36 | 0.51 | 0.56 |
| $\langle v' \rangle$ | **0.32** | 0.53 | 0.45 | 0.99 | 0.50 | 0.76 | 0.85 |
| $\langle j' \rangle$ | **1.71** | 2.27 | 2.22 | 2.05 | 4.65 | 4.71 | 4.72 |
| $\langle E_{rel} \rangle$ (eV) | **0.15** | 0.24 | 0.20 | 0.43 | 0.29 | 0.88 | 0.60 |
| Relative RMS Errors (%) | | | | | | | |
| | nr-**d** | | rot-**d** | | Ehrenfest | | |
| | ad-TFS[b] | di-TFS[c] | ad-TFS[b] | di-TFS[c] | Hist | LSS | QSS |
| $\tau$ (ps) | **47** | 79 | 51 | 48 | 286 | 75 | 90 |
| $\langle v' \rangle$ | **30** | 58 | 35 | 103 | 51 | 63 | 70 |
| $\langle j' \rangle$ | **43** | 59 | 51 | 49 | 73 | 72 | 72 |
| $\langle E_{rel} \rangle$ (eV) | **18** | 28 | 22 | 47 | 52 | 128 | 91 |

[a] Bold numbers indicate the lowest error for each of the four quantities [a] Adiabatic Tully's fewest switches algorithm. [b] Diabatic Tully's fewest switches algorithm.

**TABLE 6: Average Number of Successful Hops, Linear Momentum Prohibited Hops, and Energy Prohibited Hops Per Trajectory, Averaged Over All Energies**

| Potential Matrix 5F | | | | |
|---|---|---|---|---|
| | nr-**d** | | rot-**d** | |
| | ad-TFS[a] | di-TFS[b] | ad-TFS[a] | di-TFS[b] |
| successful hops | 7.5 | 1.1 | 8.9 | 1.1 |
| momentum failures | 0.5 | 0.3 | 0.0 | 0.0 |
| energy failures | 0.7 | 1.8 | 0.8 | 1.7 |
| Potential Matrix 6 | | | | |
| | nr-**d** | | rot-**d** | |
| | ad-TFS[a] | di-TFS[b] | ad-TFS[a] | di-TFS[b] |
| successful hops | 1.0 | 1.4 | 1.3 | 4.8 |
| momentum failures | 0.5 | 4.0 | 0.0 | 0.0 |
| energy failures | 1.6 | 17.3 | 1.3 | 21.6 |

[a] Adiabatic Tully's fewest switches algorithm. [b] Diabatic Tully's fewest switches algorithm.

diabatic coupling vanishes at $C_{2v}$ geometries, where the bottom of the exciplex well is located.

An analysis of the final decay products of the resonances for potential matrix 5F and potential matrix 6 reveals three more trends between matrices. A comparison of Figure 4 to Figure 8a−c shows that in general the average vibrational quantum number of the decay products increases as the total energy is increased for both potential matrices. On the other hand, a comparison of Figure 5 to Figure 9a−c shows that the average rotational quantum number of the decay products tends to increase with the total energy for potential matrix 5F and it tends to decrease with total energy for potential matrix 6. A comparison of Figure 6 to Figure 10a−c shows that the final relative energy of the decay products tends to decrease with total energy for potential matrix 5F, and it tends to increase with total energy for potential matrix 6. These three trends of quantities of the decay products to change with energy are less well explained by changes in the potential energy matrix.

The extent of agreement of the single-surface bound-state calculations with the fully coupled calculations depends on the choice of representation of the single surface. Table 2 shows a very strong dependence for potential matrix 5F, and Table 3 shows a weaker dependence for potential matrix 6. For potential

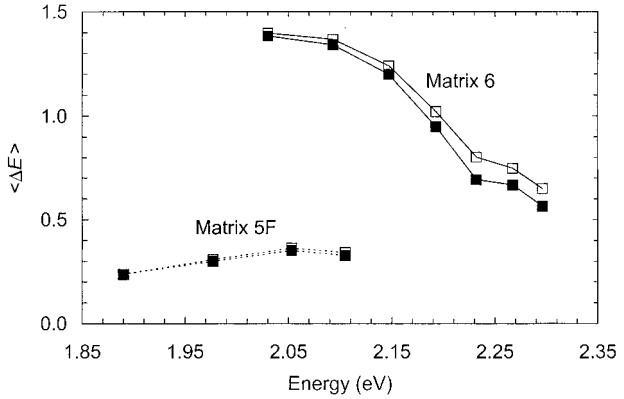


**Figure 11.** Average absolute value of the energy gap at surface hops for potential matrix 5F and potential matrix 6 versus energy. The solid squares represent the hm-TFS-nr-**d** method; the open squares represent the hm-TFS-rot-**d** method. The dashed lines represent values for potential matrix 5F; the solid lines represent values for potential matrix 6. For potential matrix 6, only the 0*n*0 resonances have been shown for clarity.

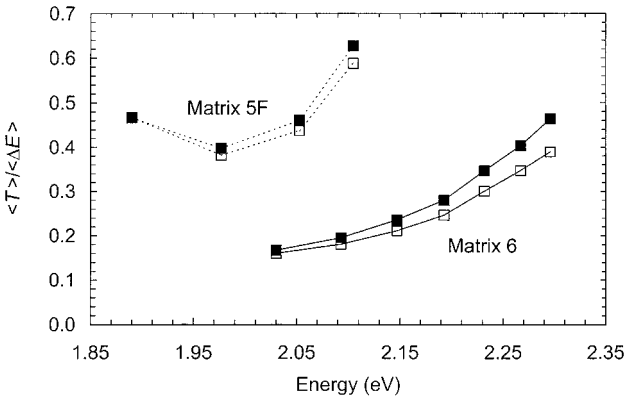


**Figure 12.** Ratio of the average kinetic energy to the average absolute value of the energy gap at surface hops for potential matrix 5F and potential matrix 6. The solid squares represent the hm-TFS-nr-**d** method; the open squares represent the hm-TFS-rot-**d** method. The dashed lines represent values for potential matrix 5F; the solid lines represent values for potential matrix 6.

matrix 5F, the diabatic single-surface calculations agree best with the fully coupled problem, while for potential matrix 6 it is the adiabatic single-surface calculations that agree best with the fully coupled problem. The dependence of the single-surface calculations on the representation is probably related to the coupling between electronic states. The single-surface calculations may be thought of as approximations to the fully coupled calculations arrived at by setting the coupling between surfaces to zero. The error of this approximation will thus be the smallest when the single surface is in the representation that has the smallest interstate coupling. The diabatic coupling vanishes at $C_{2v}$ geometries and is small at non-$C_{2v}$ geometries near the exciplex well for both potential matrices. On the other hand, potential matrix 5F has much larger nonadiabatic coupling than potential matrix 6 does in energetically accessible regions, as described above. This large nonadiabatic coupling for potential matrix 5F explains why the diabatic representation of the single surface best agrees with the fully coupled calculation. For potential matrix 6, the difference in the two representations is not as important as evidenced by the slight differences in representation shown in Table 3. However, the inaccessibility of the line of conical intersections is evidently a more important factor than the nonzero diabatic coupling at non-$C_{2v}$ geometries.

Our third criterion thus predicts that the adiabatic representa-

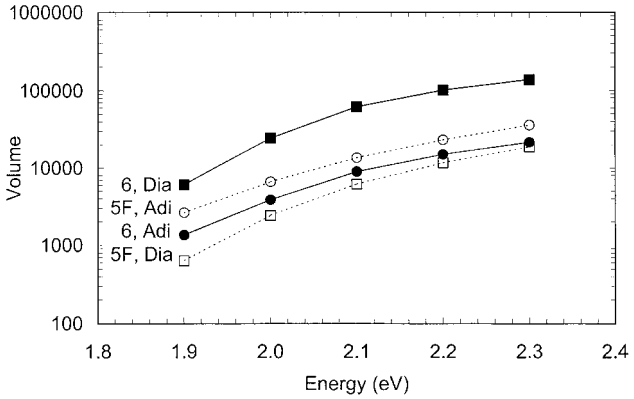


**Figure 13.** Diabatic and nonadiabatic coupling volume for potential matrix 5F and potential matrix 6 versus the total energy. The squares represent diabatic coupling volume, and the circles represent adiabatic coupling volume. The open symbols linked by dashed lines represent values for potential matrix 5F; the filled symbols linked by solid lines represent values for potential matrix 6.

tion will be the best for trajectory surface hopping methods for potential matrix 6, while the diabatic representation will be the best for potential matrix 5F.

In summary, differences in three of the six trends are explainable in terms of differences in the potential matrices, but differences in the other three are less well explained. One goal of our comparisons of semiclassical calculations to quantum mechanical calculations is to be able to further explain the quantum mechanical results with a semiclassical interpretation. For instance, although the trends in the final vibrational and rotational quantum numbers and the final relative energy were not easily explainable in terms of features of the potential energy matrix, we may be able to describe them semiclassically. However, the semiclassical explanations are valid only to the extent that they reproduce the accurate quantum calculations for each potential matrix. We examine this issue next.

**6.2. Comparison of Semiclassical Trajectory Surface Hopping Calculations to Quantum Mechanical Calculations for Each Potential Energy Matrix.** Of the six trends described in the previous section, the semiclassical methods make predictions for all except the resonance energies (since we carried out our semiclassical calculations at the quantum mechanical resonance energies, the semiclassical calculations reproduce the energy spacings by construction). The errors in the semiclassical methods for the quantities, averaged over all of the resonances, are shown in Tables 4 and 5. We first discuss the accuracy of the semiclassical trajectories for potential matrix 5F, and then we discuss the accuracy of the trajectories for potential matrix 6. Finally, we examine two criteria for predicting the accuracy of a semiclassical calculation from trajectory calculations.

*6.2.1. Potential Matrix 5F.* Figure 3 shows that the lifetimes predicted by the diabatic-TFS-**d** methods and the Ehrenfest methods agree qualitatively with the accurate quantum mechanical lifetimes much better than the lifetimes predicted by adiabatic-TFS-**d** methods do. The diabatic-TFS-**d** methods are the hop-minimizing methods for this potential matrix, and they have the lowest error of all of the semiclassical methods. It is interesting to note that both the rotated and nonrotated variants in the diabatic representation give nearly identical results (Figure 3). The rotated and nonrotated variants of the adiabatic-TFS-**d** method, however, predict different lifetimes.

In the calculations of the average final vibrational quantum number, all of the semiclassical methods correctly predict that $\langle v' \rangle$ will be higher for higher-energy initial states (Figure 4). The diabatic-TFS-**d** methods have the smallest error; the adiabatic trajectory surface hopping method and the Ehrenfest method predict an average final vibrational quantum number that is too low.

In the calculations of the average final rotational quantum number, on the other hand, the adiabatic-TFS-nr-**d** method shows the lowest error. All of the semiclassical methods predict a similar trend of $\langle j' \rangle$ to increase as the energy of the initial state is increased (Figure 5).

All of the trajectory surface hopping methods predict that the relative energy of the products decreases as the energy of the initial state is increased (Figure 6). However, the diabatic-TFS-**d** methods have a much smaller error than the adiabatic-TFS-**d** methods do. The Ehrenfest methods not only have a large error, but they also predict that the relative energy increases as the energy of the initial state is increased, except for the 100 state.

Overall, the diabatic-TFS-**d** trajectory calculations show the best agreement with the quantum mechanical calculations, and the rotation of the hopping vector has little effect on the final results for this method. The adiabatic calculations are much poorer (except for $\langle j' \rangle$). The surface hopping trajectories thus agree with the quantum mechanical single-surface bound-state calculations in showing that the diabatic representation is superior for potential matrix 5F. All three of our criteria thus predict correctly which choice of representation is most appropriate for surface hopping calculations with potential matrix 5F. The Ehrenfest method usually has intermediate accuracy between the adiabatic and the diabatic surface hopping methods. Unlike the surface hopping methods, however, the Ehrenfest method is independent of electronic representation, and thus, as pointed out in section 3.2, there are no electronic representation issues with this method.

*6.2.2. Potential Matrix 6.* For potential matrix 6, the lifetimes predicted by the adiabatic surface hopping methods typically agree with the accurate quantum mechanical lifetimes better than the those predicted by the diabatic ones. Note that for potential matrix 6, the adiabatic representation is the hop-minimizing representation. It can be seen in Figure 7a−c that the diabatic surface hopping methods all underestimate the mean lifetime. Another trend that is evident in Figure 7a−c is that the rotated vector methods predict a lifetime that is longer than the predictions of the corresponding nonrotated vector methods. All of the adiabatic surface hopping methods and the Ehrenfest methods show a tendency for the calculated lifetime to decrease as the energy of the initial state is increased, as can be seen in Figure 7a−c. The accurate quantum mechanical lifetimes, however, do not systematically decrease as energy is increased. Instead, in the 0*n*0 and 00*n* series the accurate lifetime increases with energy, while in the going from the 000 state to the 100 state the accurate lifetime decreases. In an earlier paper,[16] we noted a correlation between a trend of the surface hopping lifetimes to decrease with initial energy and a trend in the quenching probability to decrease with increasing energy of the initial state. In that paper we were concerned only with the 0*n*0 series, whose initial momentum is largely directed along the $R_{Na-H_2}$ coordinate. Some trajectories starting in 0*n*0 states with energies larger than 2.104 eV (the classical asymptotic energy) dissociated on the excited potential energy surface rather than quench, although this violates zero-point energy conservation. We hypothesized that preventing the trajectories from violating zero-point energy conservation would increase the mean lifetime.

In comparing the results for the 100 state to those for the 000 state, the adiabatic surface hopping methods and the

Ehrenfest method agree with the accurate quantum mechanical calculations in that they predict a decrease in the lifetime for 100. One may wonder whether this agreement is accidental and if the nonconservation of zero point energy by the semiclassical methods is responsible for the short lifetime of the 100 state. However, there is evidence that suggests that zero point energy conservation is not as important a factor in the semiclassical lifetime calculations for the 100 state as it is for the 0*n*0 series. In the 100 state, most of the momentum is directed along the $r_{H_2}$ coordinate instead of toward the Na(3p) + $H_2$ asymptote. The $r_{H_2}$ coordinate is roughly perpendicular to the line of avoided crossings, where the nonadiabatic coupling is the strongest. Thus, trajectories are more likely to quench before their momentum can be redistributed and before they dissociate on the upper surface. The quenching probability for the 100 resonance calculated by the adiabatic-TFS-nr-**d** method is 0.71, while the quenching probability for the 060 resonance calculated by the adiabatic-TFS-nr-**d** method is 0.40. Therefore, when the conservation of zero-point energy is not a strong factor, the adiabatic TFS methods do give qualitative agreement with the accurate quantum mechanical lifetimes. Similar arguments may be applied to the Ehrenfest method, except that in this case quenching is less well defined. Instead of occurring at a single location, the process of quenching in the Ehrenfest method occurs more gradually, as can be seen in eqs 3 and 9. We still expect that the motion of an Ehrenfest trajectory across the line of avoided crossings will be more effective at transforming the self-consistent potential of eq 9 into a potential similar to the ground state than motion along the $R_{Na-H_2}$ coordinate will.

All of the TFS methods and the Ehrenfest variants predict a final average vibrational quantum number that increases with an increase in energy of the initial states. In Figure 8a−c it can be seen that the accurate quantum mechanical vibrational numbers also increase with the energy of the initial state, except for the 002 state. As we discussed in an earlier paper,[16] lower-energy trajectories are energetically unable to cross the conical intersection for this potential matrix. As energy is increased, a larger region of the potential surface becomes energetically accessible to trajectories, and at 2.06 eV the conical intersection itself becomes accessible. The component of the nonadiabatic coupling vector along the $H_2$ vibrational mode is largest near the conical intersection, and since the **d** vector (or a rotated variant) is used to adjust the momentum of trajectories during surface hops, high-energy trajectories form products with higher vibrational excitation. The trend of the accurate quantum mechanical vibrational quantum numbers to increase with increasing energy is therefore qualitatively described by trajectories hopping near the conical intersection using the **d** vector. This explanation also applies to the Ehrenfest method; the self-consistent potential changes more rapidly as Ehrenfest methods approach the conical intersection. However, the surface hopping model provides a clearer picture of the nonadiabatic process than does the Ehrenfest method.

The adiabatic-TFS-**d** methods best reproduce the accurate quantum mechanical trend of the final average rotational quantum number to decrease as the energies of the initial states are increased (Figure 9a−c). The component of the nonadiabatic coupling vector along the bending coordinate is smallest near the conical intersection, and so high energy trajectories will form products that have smaller rotational quantum numbers. All three Ehrenfest methods underestimate the final average rotational quantum number.

The Ehrenfest method overestimates the amount of relative energy of the products. The other semiclassical methods all agree well with the quantum mechanical relative energies by comparison (Figure 10a−c). For example, the adiabatic-TFS-**d** method has a relative error of 18%, the diabatic-TFS-**d** method has a relative error of 28%, and the Ehrenfest-Hist has a relative error of 52%. More detailed comparisons are shown in Table 5.

The adiabatic trajectories have good agreement with the quantum mechanical calculations for the trends in the average final quantum numbers of the decay products. Note that diabatic trajectories do not necessarily hop near the conical intersection, since the diabatic surfaces are coupled by the off-diagonal coupling element, which is very small near the conical intersection. Thus, diabatic TFS trajectories do not predict final vibrational and rotational quantum numbers that have the same dependence on the energy of the initial state that the adiabatic TFS trajectories do. The extent that the adiabatic TFS methods describe the final average rotational and vibrational quantum numbers better than the diabatic TFS methods do implies that the adiabatic representation is more appropriate for trajectory surface hopping calculations for potential matrix 6. Further evidence of the superiority of the adiabatic representation for potential matrix 6 is that surface hopping calculations in the adiabatic representation have smaller overall errors than calculations in the diabatic representation do. For this potential matrix, all three criteria for the selection of the best trajectory representation are successful.

*6.2.3. Criteria for Determining the Overall Accuracy of a Semiclassical Calculation.* Beyond determining which representation will be the most accurate for semiclassical calculations, it would be useful to be able to predict the size of the absolute error in the semiclassical methods from dynamical information. Note, for example, that the overall error in the hm-TFS-nr-**d** method for potential matrix 5F is much smaller than the overall error in the hm-TFS-nr-**d** method for potential matrix 6. We checked two different criteria for the absolute accuracy of the semiclassical methods. The first is the size of the average energy gap during surface hops. The average gap is illustrated in Figure 11 for potential matrices 5F and 6. The average energy gap of trajectories for potential matrix 5F is much smaller than the average energy gap of trajectories for potential matrix 6. The correlation between the size of the hopping gap and the size of the error of the hm-TFS-nr-**d** method suggests that the direction of the hopping vector may be crucial to an accurate description of reaction dynamics, especially for systems with large energy gaps. This is because large energy gaps require large adjustments to the kinetic energy, and the final energy distributions are determined largely by the redistribution of momentum during a hop. The present calculations confirm our earlier observations[13,16] that for potential matrix 5F, both the hm-TFS-rot-**d** method and the hm-TFS-nr-**d** method produced similar energy distributions in the final trajectory states, while for potential matrix 6 the difference in the two methods is larger (Tables 4 and 5).

Another criterion that has been suggested[19] for assessing the accuracy of trajectory calculations is the ratio of the kinetic energy to the size of the energy gap during hopping events. This ratio is generally larger for the hm-TFS-nr-**d** method for potential matrix 5F than it is for the hm-TFS-nr-**d** method for potential matrix 6 (Figure 12). This confirms that a greater fraction of the final kinetic energy is partitioned during surface hopping for potential matrix 6 than for potential matrix 5F.

**6.3. Which Semiclassical Trajectory Method, the Surface Hopping Method or the Self-Consistent Potential Method, Best Describes Each Potential Matrix?** For potential matrix

5F, the Ehrenfest calculations have intermediate accuracy between the diabatic and the adiabatic surface hopping calculations, typically slightly better than the adiabatic calculations and worse than the diabatic calculations. The only exception to this is the average final rotational quantum number, for which the adiabatic surface hopping method is the best, followed by the Ehrenfest and then by the diabatic method. All three kinds of trajectory methods reproduce trends of the lifetimes, average final rotational quantum numbers, and average final vibrational quantum numbers to change with a change in the total energy. However, the Ehrenfest method does not reproduce the trend of the average final relative energy as a function of total energy, while both representations of the trajectory surface hopping method do. Overall, Table 4 shows that the diabatic trajectory surface hopping calculations are the most accurate, while the adiabatic trajectory surface hopping calculations and the Ehrenfest method have larger errors.

These findings are consistent with earlier work[13] that showed that the Ehrenfest method typically worked as well as the adiabatic trajectory surface hopping method.

The Ehrenfest calculations have higher overall errors than either of the surface hopping calculations do for potential matrix 6. The Ehrenfest method far underestimates the amount of final rotational excitation in the products and overestimates the amount of relative energy in the products. It does, however, correctly predict the trend of the average final vibrational number to increase with energy, and the error of the Hist-Ehrenfest method for the vibrational quantum number is slightly smaller than the diabatic surface hopping method.

One reason that the Ehrenfest methods may do better for potential matrix 5F than they do for potential matrix 6 is that the states are more strongly coupled in potential matrix 5F. The conical intersection in potential matrix 5F, for instance, is energetically accessible at low energies. During the calculation of Ehrenfest trajectories, the self-consistent potential rapidly changes from resembling an excited-state potential surface to resembling a ground-state potential surface in regions of strong coupling. For potential matrix 5F, the average squared final excited-state coefficient for the self-consistent potential for trajectories starting in the 000 state is 0.31. On the other hand, for potential matrix 6, the state coupling is much weaker. The self-consistent potential only gradually changes for this potential matrix, and once the asymptotic region of the average potential becomes energetically accessible, the exciplexes dissociate. The average squared excited-state coefficient is 0.85 for trajectories starting in the 000 state for potential matrix 6. Thus, it may not be too surprising that for potential matrix 6 the Ehrenfest method does not accurately describe the ground-state decay products.

Overall, the surface hopping calculations describe the quantum mechanics more closely than the Ehrenfest method does for either potential matrix.

**6.4. Do the Semiclassical Methods Reproduce the Trends Shown by the Quantum Mechanical Calculations between the Two Potential Matrices?** By construction, the trajectory calculations all reproduce the quantum mechanical resonance energy spacings for both potential matrices.

The adiabatic trajectory surface hopping calculations and the Ehrenfest calculations both show an increase in the calculated lifetimes in going from potential matrix 5F to potential matrix 6, in agreement with the quantum calculations (Figures 3 and 7a−c). The diabatic trajectory surface hopping calculations, however, do not show this trend. An examination of Figures 3 and 7a−c shows that the diabatic trajectory lifetimes for potential matrix 5F agree well with the quantum mechanical calculations, but the diabatic trajectories for potential matrix 6 are much too short.

For both potential matrices, the quantum mechanical calculations show that the average final vibrational quantum number increases as the total energy is increased. All of the semiclassical trajectory calculations reproduce this trend.

In potential matrix 5F, the quantum mechanical calculations show that the average final rotational quantum number increases as the total energy is increased. On the other hand, in potential matrix 6 the quantum mechanical prediction of the average final rotational number decreases as the total energy is increased. The only semiclassical calculation to reproduce this behavior of the average final rotational quantum number is the adiabatic trajectory surface hopping method.

In potential matrix 5F, the quantum mechanical calculations show that the final relative translational energy decreases with total energy, whereas in potential matrix 6 the quantum mechanical calculations show that the relative energy increases with total energy. Both the adiabatic and the diabatic trajectory surface hopping methods reproduce this trend, but the Ehrenfest method does not.

When one uses the hop-minimizing representation, the semiclassical surface hopping calculations correctly reflect the trend of the change in lifetimes, the change in average final quantum numbers, and the change in relative energy between potential matrices. Furthermore, the hm-TFS calculations have the smallest overall error of all of the semiclassical methods for both potential matrices.

The last trend we examine between potential matrix 5F and potential matrix 6 is the superiority of a particular electronic representation. The surface hopping trajectories reproduce the quantum mechanical preference for resonances on potential matrix 6 to be best described by an adiabatic representation and for resonances on potential matrix 5F to be described by a diabatic representation. All three of our criteria correctly predict the best representation for the trajectory surface hopping calculations.

## 7. Conclusions

We have presented quantum mechanical calculations for the Feshbach funnel resonances of two different $NaH_2$ potential energy matrices called 5F and 6. These calculations provide accurate decay lifetimes and branching probabilities for each of the given potential matrices. Some of the differences in the results of the coupled quantum mechanical calculations for these potential matrices have been correlated with features of the potential matrices. For example, the spacings of the resonance energies are correlated with the shape of the exciplex well. The lifetimes of the resonances are correlated with the magnitude of the nonadiabatic coupling in regions of high wave function density.

The extent of agreement of single-surface bound state quantum mechanical calculations with the fully coupled quantum mechanical calculations depends on the choice of representation of the single surface. For $NaH_2$ potential matrix 5F, diabatic single-surface calculations agree best with the fully coupled calculations, while for $NaH_2$ potential matrix 6 it is the adiabatic single-surface calculations that agree best. The dependency of the agreement on the representation is correlated with the location of the line of conical intersections relative to the exciplex well.

We performed semiclassical trajectory methods both with the surface hopping method and with the Ehrenfest method. The surface hopping calculations used Tully's fewest switches (TFS)

method and were carried out in both the adiabatic and the diabatic representation. The semiclassical trajectory calculations show some of the same trends that the quantum mechanical calculations show with respect to changing potential energy matrices. For example, the lifetimes of the trajectories are much shorter for potential matrix 5F than they are for potential matrix 6.

The trajectory surface hopping calculations may be performed in either the adiabatic or diabatic representation. We tested three criteria for predicting which representation will be most accurate. According to our first criterion, we calculate trajectories in both representations and accept the results of the representation that has the fewest average number of surface hops. A drawback of this criterion is that two sets of dynamics calculations must be performed, increasing the computational expense. Our second criterion requires no dynamical information but only requires the evaluation of two integrals over the energetically accessible regions of phase space. The representation that has the smallest coupling volume (defined in section 3.3) is the appropriate representation to perform trajectory surface hopping calculations. The third criterion is to compare fully coupled quantum mechanical calculations with single-surface quantum mechanical calculations. The representation of the single surface that agrees best with the fully coupled calculations should be used in surface hopping calculations. For large systems, this criterion is not very useful because it requires converged quantal calculations, which are only practical for small systems. We note that all three criteria gave identical predictions for the best representation.

When we used the representation for each potential energy matrix that minimizes the number of hops, we found that the trajectory surface hopping calculations show qualitative agreement with the quantum mechanical calculations for potential matrix 6, and they show even better agreement with the quantum mechanical calculations for potential matrix 5F. The average energy gap at hopping is correlated with this agreement. Semiclassical calculations in the hop-minimizing representation for potential matrix 5F predict a smaller average energy gap for hopping events than calculations in the hop-minimizing representation for potential matrix 6 do.

We examined the accuracy of the trajectory surface hopping calculations with two different choices for the vector along which the momentum of the trajectories was adjusted during surface hops. These two choices are the nonadiabatic coupling vector and another vector that is derived by allowing the nonadiabatic coupling vector to rotate to reduce the number of momentum-prohibited surface hops. We found that in general the nonadiabatic vector is the best vector to use for hopping events and that using the rotated hopping vector led to trajectories that had slightly larger errors in the final calculated quantities.

The Ehrenfest calculations have higher overall errors than the surface hopping calculations do. For potential matrix 6 the Ehrenfest calculations tend to be worse than the surface hopping calculations in either representation, while for potential matrix 5F the Ehrenfest calculations tend to be more accurate than the adiabatic surface hopping calculations but less accurate than the diabatic surface hopping calculations. For both potential matrices, the Ehrenfest calculations tend to be worse than the surface hopping calculations if the latter are based on the representation that minimizes the number of surface hops. We note that for potential matrix 5F, all three methods of analyzing the Ehrenfest results (histogramming, linear smooth sampling, and quadratic smooth sampling) gave similar results. For potential matrix 6, on the other hand, the histogram method tends to have the smallest errors except in the calculation of the lifetime, for which the linear smooth sampling method has the smallest error.

For $NaH_2$ potential matrix 5F, the best overall semiclassical method is Tully's fewest switches method in the diabatic representation using the nonadiabatic coupling vector for hopping, while for $NaH_2$ potential matrix 6 the best overall semiclassical method is Tully's fewest switches method in the adiabatic representation using the nonadiabatic coupling vector for hopping. These calculations provide clear evidence that the adiabatic representation is not always superior to the diabatic representation and that similar systems may differ in which representation is better.

It is instructive to review recent calculations comparing semiclassical and quantum mechanical calculations. Except in recent work on the collinear NaFH system,[15] all of our earlier semiclassical calculations on a variety of systems[13−16] have qualitatively agreed with accurate quantum mechanical calculations. This agreement occurs in bimolecular collisions on systems with strong coupling and with energetically accessible conical intersections,[13] in bimolecular collisions for a system with very weak coupling,[14] and in the current unimolecular decay calculations on potential matrices of with conical intersections of varying energetic accessibility.[16] This last mentioned example is especially encouraging, since it models an essentially quantum mechanical phenomenon.

Our results here and in refs 13, 14, and 16 show that among the semiclassical methods we have examined, Tully's fewest switches method is the best on average. For the weakly coupled $BrH_2$ system,[14] Tully's fewest switches method was found to have the smallest error, and the Ehrenfest method was slightly less accurate. For the earlier study of bimolecular collisions for model $MH_2$ systems,[13] Tully's fewest switches method in the adiabatic representation and the Ehrenfest methods had similar accuracy. The line of conical intersections is energetically accessible in both of these model systems, and the nonadiabatic coupling vector is very large near the conical intersection. The current work suggests that fewer surface hops would occur in the diabatic representation for the model $MH_2$ systems and that therefore diabatic-TFS calculations would be the most accurate for these systems; this prediction remains untested. For the systems studied in the current work, Tully's fewest switches method in the representation that minimizes the number of surface hops is more accurate than the Ehrenfest method. Although we have not exhausted all of the possible types of potential energy surfaces, the evidence that we have so far examined suggests that for general three-dimensional two-state systems, Tully's fewest switches method is the most accurate semiclassical method currently available if one uses the nonrotated nonadiabatic coupling vector as the hopping vector and propagates the trajectories in the representation that minimizes the number of surface hops.

Finally, we close by considering the question in the title of this paper. The average relative RMS error of the seven semiclassical methods studied here for the four final observables (lifetimes, vibrational and rotational quantum numbers of fragments, and relative translational energy of fragments) of two systems is 45%, which is an average of 23% for the more strongly coupled system 5F (which has an average lifetime of 0.2 ps) and 68% for the less strongly coupled system 6 (which has an average lifetime of 0.7 ps). However, choosing the representation for the trajectory surface hopping calculations as the one that minimizes the number of hops yields a method with an average relative RMS error of only 18% for system 5F

and 35% for system 6 for an overall average of 26%. Especially when one considers that the errors in lifetimes are potentially unbounded (unlike the other three observables, lifetimes are not constrained to finite ranges by conservation of energy or angular momentum), one would have to conclude that the accuracy is reasonable, and the answer to the title question is a guarded "yes".

**Acknowledgment.** This work was supported in part by the National Science Foundation under grant no. CHE97-25965.

## Appendix A

The evaluation of the integrals in eqs 10 and 11 is accomplished through Monte Carlo integration techniques. Since we are using Jacobi coordinates, the integrals in eqs 10 and 11 are 12-dimensional. We write the vector **R** as a combination of **s**, the vector pointing from atom B to atom C, and **S**, a vector pointing from atom A to the center of mass of BC. We further define two mass-weighted vectors

$$\mathbf{Q} = \sqrt{\mu_S}\mathbf{S} \tag{A-1}$$

$$\mathbf{q} = \sqrt{\mu_S}\mathbf{s} \tag{A-2}$$

where $\mu_s$ and $\mu_S$ are the masses associated with the vectors **s** and **S**. The momenta conjugate to these mass-weighted vectors are

$$\mathbf{P_Q} = \frac{\mathbf{P_S}}{\sqrt{\mu_S}} \tag{A-3}$$

$$\mathbf{P_q} = \frac{\mathbf{P_s}}{\sqrt{\mu_s}} \tag{A-4}$$

so that

$$\dot{\mathbf{Q}} = \mathbf{P_Q} \tag{A-5}$$

$$\dot{\mathbf{q}} = \mathbf{P_q} \tag{A-6}$$

Working in mass-scaled coordinates simplifies the calculations.

We note that the integrands of eqs 10 and 11 depend only on the internal coordinates and not on the orientation of the system in fixed space. This suggests that by a suitable coordinate transform we may remove three dimensions from the calculation.

We first consider the integral in eq 10, noting that much of the following simplification will also apply to eq 11. We may express the coordinates in eq 10 in spherical polar Jacobi coordinates as follows:

$$W_{\mathrm{dia}}(E) = \int_{\mathbf{Q}}\int_{\mathbf{q}}\int_{\mathbf{P_Q}}\int_{\mathbf{P_q}} |V_{21}(Q,q,\chi)/\hbar|\, \mathrm{d}\mathbf{Q}\, \mathrm{d}\mathbf{q}\, \mathrm{d}\mathbf{P_Q}\, \mathrm{d}\mathbf{P_q} \tag{A-7}$$

$$\mathrm{d}\mathbf{Q}\, \mathrm{d}\mathbf{q} = q^2\, \mathrm{d}q\, \sin\theta_q\, \mathrm{d}\theta_q\, \mathrm{d}\phi_q\, Q^2\, \mathrm{d}Q\, \sin\theta_Q\, \mathrm{d}\theta_Q\, \mathrm{d}\phi_Q \tag{A-8}$$

where we have defined the angles $\theta_Q$ and $\phi_Q$ with respect to an arbitrary axis $z$ in space, and we have defined the angels $\theta_q$ and $\phi_q$ with respect to the vector **Q**. With these definitions, $\theta_q$ is equal to $\chi$, the angle between **q** and **Q**, and the angles $\theta_Q$, $\phi_Q$, and $\phi_q$ orient the ABC system in space. Since the integrand does not depend on this orientation, these three angles can be factored out and eq A-7 can be written

$$W_{\mathrm{dia}}(E) = \int_{\theta_Q\phi_Q}\sin\theta_Q\, \mathrm{d}\theta_Q\, \mathrm{d}\phi_Q \int_{\phi_q}\mathrm{d}\phi_q \int_Q\int_q\int_\chi\int_{\mathbf{P_Q}}\int_{\mathbf{P_q}} |V_{21}(Q,q,\chi)/\hbar|\, \sin\chi\, \mathrm{d}\chi\, q^2\, \mathrm{d}q\, Q^2\, \mathrm{d}Q\, \mathrm{d}\mathbf{P_Q}\, \mathrm{d}\mathbf{P_q} \tag{A-9}$$

$$W_{\mathrm{dia}}(E) = 8\pi^2 \int_Q\int_q\int_\chi\int_{\mathbf{P_Q}}\int_{\mathbf{P_q}} |U_{21}(Q,q,\chi)/\hbar|\, \sin\chi\, \mathrm{d}\chi\, q^2\, \mathrm{d}q\, Q^2\, \mathrm{d}Q\, \mathrm{d}\mathbf{P_Q}\, \mathrm{d}\mathbf{P_q} \tag{A-10}$$

We then define three new coordinates:

$$X = {}^1\!/_3 Q^3 \tag{A-11}$$

$$Y = {}^1\!/_3 q^3 \tag{A-12}$$

$$\eta = -\cos\chi \tag{A-13}$$

in terms of which eq A-10 may be written

$$W_{\mathrm{dia}}(E) = 8\pi^2 \int_X\int_Y\int_\eta\int_{\mathbf{P_Q}}\int_{\mathbf{P_q}} |U_{21}(X,Y,\eta)/\hbar|\, \mathrm{d}X\, \mathrm{d}Y\, \mathrm{d}\eta\, \mathrm{d}\mathbf{P_Q}\, \mathrm{d}\mathbf{P_q} \tag{A-14}$$

The integral over the momenta may also be simplified. In particular, at any geometry R, the total momenta may be partitioned into internal-vibrational motion as well as external-rotational motion.[16] By considering cases where the total angular momenta is zero, we may reduce the dimension of the integral (A-14) by 3 and integrate over only the three internal-vibrational degrees of freedom. We then write

$$W_{\mathrm{dia}}(E) = 8\pi^2 \int_X\int_Y\int_\eta\int_{\mathbf{P}_{\mathrm{int}}} |V_{21}(X,Y,\eta)/\hbar|\, \mathrm{d}\mathbf{P}_{\mathrm{int}}\, \mathrm{d}X\, \mathrm{d}Y\, \mathrm{d}\eta \tag{A-15}$$

where $\mathbf{P}_{\mathrm{int}}$ refers to the three internal vibrational modes of the system. One final dimension may be removed by recognizing that in order for total energy to be conserved, the kinetic energy at any given geometry $X$, $Y$, $\eta$ must be given by

$$T(X,Y,\eta) = E - V(X,Y,\eta) \tag{A-16}$$

where we have defined $V(X,Y,\eta)$

$$V(X,Y,\eta) = {}^1\!/_2\, (V_{11}(X,Y,\eta) + V_{22}(X,Y,\eta)) \tag{A-17}$$

We transform to spherical polar coordinates in the momenta:

$$P_1 = P_{\max}\sin\theta_p\cos\phi_p \tag{A-18}$$

$$P_2 = P_{\max}\sin\theta_p\sin\phi_p \tag{A-19}$$

$$P_3 = P_{\max}\cos\theta_p \tag{A-20}$$

where $P_1$, $P_2$, and $P_3$ are the internal mass-weighted vibrational momenta.

$$T = \frac{1}{2}P_1{}^2 + \frac{1}{2}P_2{}^2 + \frac{1}{2}P_3{}^2 \tag{A-21}$$

$$T = \frac{1}{2}P_{\max}{}^2 \tag{A-21}$$

$$\mathrm{d}P_1\, \mathrm{d}P_2\, \mathrm{d}P_3 = P_{\max}{}^2\, \mathrm{d}P_{\max}\, \sin\theta_p\, \mathrm{d}\theta_p\, \mathrm{d}\phi_p \tag{A-23}$$

We reduce the dimension of eq A-15 by not integrating over the coordinate $\mathrm{d}P_{\max}$ (in order to conserve total energy). This gives

$$W_{\mathrm{dia}}(E) = 8\pi^2 \int_X \int_Y \int_\eta \int_{\theta_p} \int_{\phi_p} |V_{21}(X,Y,\eta)/\hbar| 2T \sin\theta_p \, \mathrm{d}\theta_p \, \mathrm{d}\phi_p \, \mathrm{d}X \, \mathrm{d}Y \, \mathrm{d}\eta \quad \text{(A-24)}$$

We define

$$\eta_p = -\cos\theta_p \quad \text{(A-25)}$$

Giving finally

$$W_{\mathrm{dia}}(E) = \frac{16\pi^2}{\hbar} \int_X \int_Y \int_\eta \int_{\eta_p} \int_{\phi_p} |U_{21}(X,Y,\eta)| (E - V(X,Y,\eta)) \, \mathrm{d}\eta_p \, \mathrm{d}\phi_p \, \mathrm{d}X \, \mathrm{d}Y \, \mathrm{d}\eta \quad \text{(A-26)}$$

The quantitiy $W_{\mathrm{dia}}(E)$ has units of

$$(a_0\sqrt{\mu})^6 (\hbar/(a_0\sqrt{\mu}))^2 (\hbar/E_{\mathrm{h}})^{-1} = a_0{}^4 \hbar E_{\mathrm{h}} \mu^2 \quad \text{(A-27)}$$

since we have integrated inverse time over all six coordinates and two momenta.

A similar simplification may be performed on eq 11. The final integral becomes

$$W_{\mathrm{adi}}(E) = 16\pi^2 \int_X \int_Y \int_\eta \int_{\eta_p} \int_{\phi_p} |\mathbf{d}_{21}(X,Y,\eta) \cdot \mathbf{v}(\eta_p,\phi_p)| T(X,Y,\eta) \, \mathrm{d}\eta_p \, \mathrm{d}\phi_p \, \mathrm{d}X \, \mathrm{d}Y \, \mathrm{d}\eta \quad \text{(A-28)}$$

where **v** is the internal velocity vector. The units of eq A-28 are also given by eq A-27.

## References and Notes


(1) Herzberg, G. *Molecular Spectra and Molecular Structure. III. Electronic Spectra and Electronic Structure of Polyatomic Molecules*; Van Nostrand Reinhold: New York, 1966; Chapter 4.

(2) Jortner, L.; Rice, S.; Hochstrasser, R. M. *Adv. Photochem*. **1969**, *7*, 149.

(3) Yardley, J. T. *Introduction to Molecular Energy Transfer*; Academic Press: New York, 1980; Chapter 9.

(4) Simons, J. *Energetic Principles of Chemical Reactions*; Jones and Bartlett: Boston, 1983; Chapter 6.

(5) Turro, N. J. *Modern Molecular Photochemistry*; University Science Books: Mill Valley, CA, 1991; Chapter 6.

(6) Teller, E. *J. Phys. Chem*. **1937**, *41*, 109.

(7) See, e.g.: Zimmerman, H. E. *J. Phys. Chem. A* **1998**, *102*, 5616 and references 2b and 22−24 therein.

(8) Klessinger, M.; Michl, J. *Excited States and Photochemistry of Organic Molecules*; VCH: New York, 1995; Chapter 4.

(9) Halvick, P.; Truhlar, D. G. *J. Chem. Phys*. **1992**, *96*, 2895. Schwenke, D. W.; Mielke, S. L.; Tawa, G. J.; Friedman, R. S.; Halvick, P.; Truhlar, D. G. *Chem. Phys. Lett*. **1993**, *203*, 565.

(10) Hack, M. D.; Truhlar, D. G. *J. Chem. Phys.* **1999**, *110*, 4315.

(11) Tully, J. C. *J. Chem. Phys.* **1990**, *93*, 1061.

(12) Meyer, H.-D.; Miller, W. H. *J. Chem. Phys*. **1979**, *70*, 3214. García-Vela, A.; Gerber, R. B.; Imre, D. G. *J. Chem. Phys*. **1992**, *97*, 7242.

(13) Topaler, M. S.; Allison, T. C.; Schwenke, D. W.; Truhlar, D. G. *J. Chem. Phys.* **1998**, *109*, 3321; **1999**, *110*, 687(E). See also earlier results for these systems reported in: Topaler, M. S.; Hack, M. D.; Allison, T. C.; Liu, Y.-P.; Mielke, S. L.; Schwenke, D. W.; Truhlar, D. G. *J. Chem. Phys.* **1997**, *106*, 8699. Topaler, M. S.; Allison, T. C.; Schwenke, D. W.; Truhlar, D. G. *J. Phys. Chem.* **1998**, *102*, 1666.

(14) Volobuev, Y. L.; Hack, M. D.; Schwenke, D. W.; Truhlar, D. G. *J. Phys. Chem. A* **1999**, *103*, 6225.

(15) Zeiri, Y.; Katz, G.; Kosloff, R.; Topaler, M. S.; Truhlar, D. G.; Polanyi, J. C. *Chem. Phys. Lett.* **1999**, *300*, 523.

(16) Hack, M. D.; Jasper, A. W.; Volobuev, Y. L.; Schwenke, D. W.; Truhlar, D. G. *J. Phys. Chem. A* **1999**, *103*, 6309.

(17) Müller, U.; Stock, G. *J. Chem. Phys*. **1997**, *107*, 6230.

(18) Tachikawa, H.; Hamabayashi, T.; Yoshida, H. *J. Phys. Chem*. **1995**, *99*, 16630.

(19) Tully, J. C. In *Modern Theoretical Chemistry*, *Part B*; Miller, W. H., Ed.; Plenum Press: New York, 1976.; pp 217−267.

(20) Sholl, D. S.; Tully, J. C. *J. Chem. Phys*. **1998**, *109*, 7702.

(21) Mead, C. A.; Truhlar, D. G. *J. Chem. Phys*. **1982**, *77*, 6090.

(22) Tawa, G. J.; Mielke, S. L.; Truhlar, D. G.; Schwenke, D. W. *J. Chem. Phys.* **1994**, *100*, 5751.

(23) Tawa, G. J.; Mielke, S. L.; Truhlar, D. G.; Schwenke, D. W. In *Advances in Molecular Vibrations and Collisional Dynamics*; Bowman, J. M., Ed.; JAI: Greenwich, CT, 1994; Vol 2B, pp 45−116.

(24) Mielke, S. L.; Tawa, G. J.; Truhlar, D. G.; Schwenke, D. W. *Int. J. Quantum Chem., Symp.* **1993**, *27*, 621.

(25) Simons, J. *ACS Symp. Ser*. **1984**, *263*, 3. Mielke, S. L.; Tawa, G. J.; Truhlar, D. G.; Schwenke, D. W. *J. Am. Chem. Soc*. **1993**, *115*, 6436.

(26) Schwenke, D. W. *Comput. Phys. Commun.* **1992**, *70*, 1.

(27) Porter, R. N.; Karplus, M.; Sharma, R. D. *J. Chem. Phys*. **1965**, *43*, 3259.

(28) Truhlar, D. G.; Muckerman, J. T. In *Atom-Molecule Collision Theory*; Bernstein, R. B., Ed.; Plenum: New York, 1979; pp 506−566.

(29) Miller, W. H.; McCurdy, C. W. *J. Chem. Phys*. **1978**, *69*, 5163.

(30) Preston, R. K.; Tully, J. C. *J. Chem. Phys.* **1971**, *54*, 4297.

(31) Truhlar, D. G.; Duff, J. W.; Blais, N. C.; Tully, J. C.; Garrett, B. C. *J. Chem. Phys.* **1982**, *77*, 764.

(32) Blais, N. C.; Truhlar, D. G. *J. Chem. Phys.* **1983**, *79*, 1334.

(33) Blais, N. C.; Truhlar, D. G.; Mead, C. A. *J. Chem. Phys*. **1988**, *89*, 6204.

(34) Gordon, R. G. *J. Chem. Phys*. **1966**, *44*, 3083.

(35) Blais, N. C.; Truhlar, D. G. *J. Chem. Phys*. **1976**, *65*, 5335.

(36) Truhlar, D. G. *Int. J. Quantum Chem., Symp*. **1976**, *10*, 239.

(37) Truhlar, D. G.; Reid, B. P.; Zurawski, D. E.; Gray, J. C. *J. Phys. Chem*. **1981**, *85*, 786.

(38) Bischof, C.; Carle, A. ADIFOR-version 2.0; Argonne National Laboratory and Rice University, 1998.

(39) Tully, J. C. *Faraday Discuss. Chem. Soc.* **1998**, *110*, 407.

(40) See, e.g., Cohen-Tannoudji, C.; Diu, B.; Laloë, F. *Quantum Mechanics;* John Wiley & Sons: New York, 1977; Vol. 2, Chapter 13, section C.